Journal of Molecular Structure 1153 (2018) 212–229

Contents lists available at ScienceDirect

Journal of Molecular Structure

journal homepage: http://www.elsevier.com/locate/molstruc

Synthesis, characterization and computational study of the newly synthetized sulfonamide molecule

P. Krishna Murthy [a], V. Suneetha [b], Stevan Armaković [c], Sanja J. Armaković [d], P.A. Suchetan [e], L. Giri [f], R. Sreenivasa Rao [b, *]

[a] Department of Chemistry, Bapatla Engineering College (Autonomous), AcharayaNagarjuna University Post Graduate Research Centre, Bapatla-522 102, A.P., India
[b] Department of Chemistry, Bapatla College of Arts and Sciences, Baptla-522 101, A.P., India
[c] University of Novi Sad, Faculty of Sciences, Department of Physics, Trg D. Obradovića 4, 21000 Novi Sad, Serbia
[d] University of Novi Sad, Faculty of Sciences, Department of Chemistry, Biochemistry and Environmental Protection, Trg D. Obradovića 3, 21000 Novi Sad, Serbia
[e] Department of Studies and Research in Chemistry, University College of Science, Tumkur University, Tumkur-572 103, Karnataka, India
[f] Solid State & Supramolecular Structural Chemistry Laboratory, School of Basic Sciences, Indian Institute of Technology Bhubaneswar, Bhubaneswar 751 008, India

ARTICLE INFO

Article history:
Received 14 July 2017
Received in revised form
27 September 2017
Accepted 7 October 2017
Available online 8 October 2017

Keywords:
Sulfonamide
SCXRD
Hirshfeld surface analysis
DFT calculations
Vibrational analysis

ABSTRACT

A new compound *N*-(2,5-dimethyl-4-nitrophenyl)-4-methylbenzenesulfonamide (NDMPMBS) has been derived from 2,5-dimethyl-4-nitroaniline and 4-methylbenzene-1-sulfonyl chloride. Structure was characterized by SCXRD studies and spectroscopic tools. Compound crystallized in the monoclinic crystal system with $P2_1/c$ space group $a = 10.0549$, $b = 18.967$, $c = 8.3087$, $\beta = 103.18$ and $Z = 4$. Type and nature of intermolecular interaction in crystal state investigated by 3D-Hirshfeld surface and 2D-finger print plots revealed that title compound stabilized by several interactions. The structural and electronic properties of title compound have been calculated at DFT/B3LYP/6-311G++(d,p) level of theory. Computationally obtained spectral data was compared with experimental results, showing excellent mutual agreement. Assignment of each vibrational wave number was done on the basis of potential energy distribution (PED). Investigation of local reactivity descriptors encompassed visualization of molecular electrostatic potential (MEP) and average local ionization energy (ALIE) surfaces, visualization of Fukui functions, natural bond order (NBO) analysis, bond dissociation energies for hydrogen abstraction (H-BDE) and radial distribution functions (RDF) after molecular dynamics (MD) simulations. MD simulations were also used in order to investigate interaction of NDMPMBS molecule with 1WKR and 3ETT proteins protein.

1. Introduction

SO_2—NH group is a key constituent of sulfonamide pharmaceuticals, which are promising chemotherapeutic agents used for treatment of various diseases [1]. Sulfa-drugs possess a wide verity of medicinal chemistry applications such as antiprotozoal [2], antibacterial [3], antifungal [4], insecticidal [5], anti-inflammatory [6], carbonic anhydrase inhibitor [7] and rheumatoid arthritis [8]. Recent literature reports indicate that sulphonamides are also applied in the cases of Alzheimer's [9], cancer [10,11] and HIV [12] diseases as well. Besides pharmaceutical applications, sulphonamides are also used as reagents in analytical chemistry for concentration, separation, selective qualitative and quantitative determination of the 3d transition metal cations [13–15]. Sulfonamide compounds have been studied extensively and numerous experimental and computational reports. Xing et al. reported the crystal structure of 4-methyl-*N*-(4-nitrophenyl)benzenesulfonamide [16]. Sarojini et al. reported synthesis, structural, spectroscopic and computational studies of 4-methyl-*N*-(3-nitrophenyl) benzene sulfonamide combining experimental and theoretical approaches [17]. Rajamani et al. investigated electronic absorption, vibrational spectra, nonlinear optical properties, NBO analysis and thermodynamic properties of *N*-(4-nitro-2-phenoxyphenyl) methanesulfonamide molecule within the Hartree-Fock and

* Corresponding author.
E-mail address: rsrchemhod@gmail.com (R.S. Rao).

https://doi.org/10.1016/j.molstruc.2017.10.028
0022-2860/

density functional approaches [18]. Govindarasu et al. carried out detailed experimental and computational DFT study of *N*-phenylbenzenesulfonamide [19].

In this paper we report synthesis, detailed spectroscopic and computational characterization of *N*-(2,5-dimethyl-4-nitrophenyl)-4-methylbenzenesulfonamide (NDMPMBS) molecule. In order to uniquely characterize the title compound we have measured FT-IR, Raman and NMR spectra. Spectral data were also computed within DFT approach in order to validate the used level of theory. Computational investigation within DFT approach has proven to be effective tool for investigation of physical and chemical properties of various organic molecules [20–24] and in this study we used it to study both global and local quantum-molecular descriptors of the title compound. Taking into account that organic pharmaceutical molecules such as NDMPMBS represent great threat for water resources [25–30], we have also investigated sensitivity of NDMPMBS towards autoxidation and hydrolysis, in order to gain an insight into its possible degradation properties.

2. Material and methods

2.1. General remarks

FT-IR spectrum (Fig. 1) was recorded in solid state using KBr disc in the range of 4000–600 cm^{-1} on ATR module ALPHA-T Bruker FT-IR spectrophotometer. FT-Raman spectrum (Fig. 2) was measured for solid sample on Bruker RFS 100/s, Germany using Nd:YAG laser source, excitation wave length 1064 nm with spectral resolution 2 cm^{-1} in the region of 0–4000 cm^{-1}.^{1}H and ^{13}C NMR chemical shift values were reported in ppm using TMS as internal standard on Bruker 400 MHz spectrometer.

2.2. Synthesis of N-(2,5-dimethyl-4-nitrophenyl)-4-methylbenzenesulfonamide

To a stirred solution of 2,5-dimethyl-4-nitroaniline (0.5 g, 3.01 mmol) in pyridine (5 mL), 4-methylbenzene-1-sulfonyl chloride (0.86 g, 4.51 mmol) was added. The reaction mixture was stirred for 16 h at room temperature. After completion of reaction by TLC, the reaction mixture was diluted with D.M.water and acidified with dilute HCl solution. Solid was filter, washed with D.M.water, MTBE and followed by 1:1 ethyl acetate: hexane. Dried under vacuum to afford (0.67 g, 69%) of *N*-(2,5-dimethyl-4-nitrophenyl)-4-methylbenzene-1-sulfonamide as pale yellow solid (Scheme-1 supporting information). Suitable single crystals were grown by slow evaporation solution growth technique at ambient temperature using chloroform: methanol (1:3) solvent.

2.3. X-ray data collection and refinement details

A suitable prism like crystal was selected and mounted on a Bruker APEX-II CCD diffractometer using graphite monochromated MoKa (λ = 0.71073 Å) radiation and detector (CCD). The crystal was kept at 273 (2) K during data collection. The structure was solved using Olex2 software with the olex2. solve [31] structure solution program using Charge Flipping and the structure was refined with the ShelXL [32] refinement package using Least Squares minimization. All the non-hydrogen atoms were revealed in the first difference Fourier map itself and were refined anisotropically. All the hydrogen atoms were positioned geometrically. All H atoms were positioned geometrically, with C–H = 0.96 Å for methyl H, C–H = 0.93 Å for aromatic H, and refined using a riding model with $U_{iso}(H) = 1.5U_{eq}(C)$ for methyl H and $U_{iso}(H) = 1.2U_{eq}(C)$ for aromatic H. The nitrogen bound H atom was located in a difference map and was refined isotropically with the bond length restraint N–H = 0.86 (2) Å. All the geometrical calculations were carried out using the program *PLATON* [33] within the WinGX suite [34]. The molecular and packing diagrams were generated using the software *MERCURY* [35]. The crystallographic data and refinement parameters are summarized in Table 1.

2.4. Computational details

Firstly, molecular structure of the title compound was extracted from the single crystal X-ray structure to be used as a starting geometry for geometry optimization. The molecular geometry optimization in gas phase together with vibrational analysis, frontier orbital analysis (HOMO-LUMO), MEP, surface analysis and Mullikan atomic charges calculation were performed at DFT level of theory with B3LYP [36] hybrid exchange-correlation functional and 6-311G++(d,p) (5D, 7 F) basis set, using Gaussian 09 software package [37]. The assignment and PED analysis of wave number were done by GaussView 5.0 program [38] and VEDA4 program [39]. For better agreement of calculated wavenumber number with

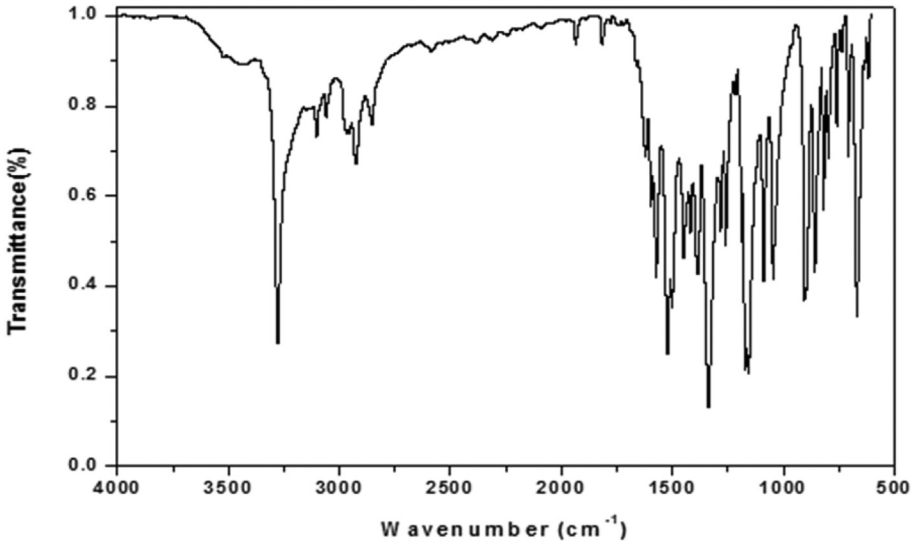

Fig. 1. FT-IR spectrum of *N*-(2,5-dimethyl-4-nitrophenyl)-4-methylbenzenesulfonamide.

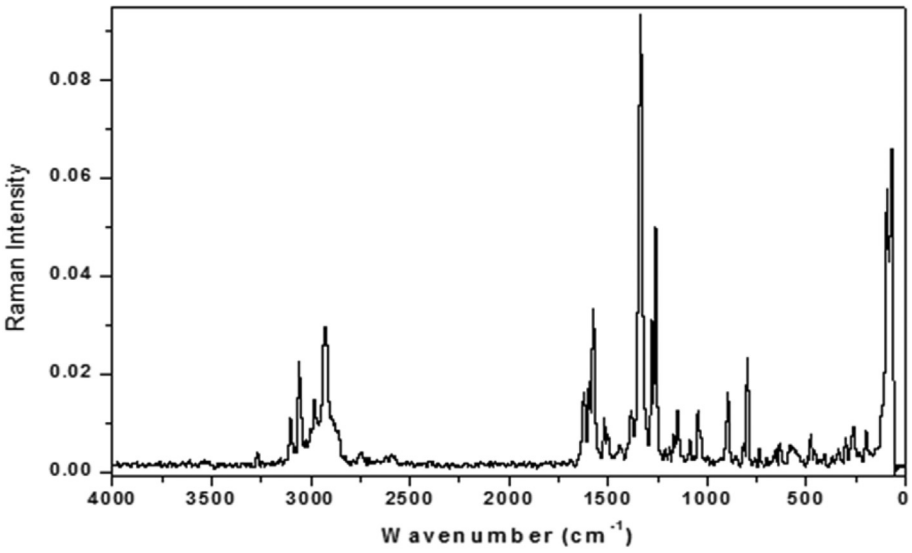

Fig. 2. FT-Raman spectrum of *N*-(2,5-dimethyl-4-nitrophenyl)-4-methylbenzene sulfonamide.

Table 1
Crystallographic data and structure refinement parameters of NDMPMBS.

CCDC Number	1539743
Empirical formula	$C_{15}H_{16}N_2O_4S$
Formula weight	320.37
Temperature/K	273.15
Crystal system	monoclinic
Space group	$P2_1/c$
a/Å	10.0549 (13)
b/Å	18.967 (2)
c/Å	8.3087 (11)
α/°	90
β/°	103.184 (4)
γ/°	90
Volume/Å^3	1542.8 (3)
Z	4
ρ_{calc}g/cm^3	1.3792
μ/mm^{-1}	0.229
F (000)	672.8
Crystal size/mm^3	0.28 × 0.25 × 0.22
Radiation	Mo Kα (λ = 0.71073)
2Θ range for data collection/°	4.68 to 53.02
Index ranges	$-12 \le h \le 12$, $-23 \le k \le 23$, $-10 \le l \le 10$
Reflections collected	28527
Independent reflections	3199 [R_{int} = 0.0493, R_{sigma} = 0.0222]
Data/restraints/parameters	3199/0/206
Goodness-of-fit on F^2	1.073
Final R indexes [I ≥ 2σ (I)]	R_1 = 0.0416, wR_2 = 0.1127
Final R indexes [all data]	R_1 = 0.0464, wR_2 = 0.1188
Largest diff. peak/hole/e Å^{-3}	0.32/-0.46

experimental values, the wave numbers were scaled by a scaling factor 0.9613 [40]. DFT calculations were also performed with Jaguar 9.6 [41] program with B3LYP functional and 6−311++G (d,p), 6-31 + G (d,p), 6-311G (d,p) basis sets for calculations of ALIE, Fukui functions and BDEs, respectively. MD simulations and RDF calculations were performed with Desmond program [42–45]. Both Jaguar and Desmond programs were used as implemented in Schrödinger Materials Science Suite 2017−2 [45]. In case of the MD simulation, one molecule of title compound was placed in the cubic box with approximately 3000 water molecule. OPLS3 force field [42,46–48] was used and the model was of NPT ensemble class. Simulation time was set to 10 ns, temperature to 300 K, pressure to 1.0325 bar, with cut-off radius set to 12 Å. Simple point charge (SPC) model [49] was used for description of solvent. An approach developed by Johnson et al. [50,51], as implemented in Jaguar program, was applied for the investigation of intra molecular non-covalent interactions.

2.5. Hirshfeld surfaces

The 3D-Hirshfeld surfaces [52–54] and the corresponding 2D-fingerprint plots (d_e *vs* d_i) [55–57], provides summary and quantification of the intermolecular interactions in the crystal structure [52,58], were generated by using CrystalExplorer3.1 [59] and which accepts a structure input file in the CIF format. The d_{norm} values are mapped onto the Hirshfeld surfaces by using a rainbow colour scheme (red-white-blue): where a red colour indicates contacts shorter than sum of van der Waals radii, white colour denotes for contacts around the *vdW* and blue colour specifies contacts longer than sum of van der Waals radii.

3. Result & discussion

3.1. Molecular and crystal structure

The *ORTEP* view of the molecule of the title compound is shown in Fig. 3. The dihedral angle between the two benzene rings in the title compound is 85.54 (6)°. The nitro group is essentially planar (rmsd = 0.003 Å) and is tilted to the aniline ring by 25.86 (3)°. The atoms around the sulfonamide S_{37} atom in the title compound are arranged in a slightly distorted tetrahedral arrangement as observed generally in sulfonamides. The biggest deviation is in the angle $O_{33}-S_{37}-O_{34}$ of 119.34 (1)°, followed by 104.14 (2)° of $O_{33}-S_{37}-N_{31}$. The V shaped molecular conformation is stabilized by intramolecular C−H···O hydrogen bonds involving H_{18} and O_{34} atoms (Fig. 3, Table 2) that encloses to form a S (6) motif. In the crystal, molecules are linked by pairs of N−H···O hydrogen bonds involving amino nitrogen atom N_{31} as the hydrogen bond donor and sulfonyl oxygen atom O_{33} as the acceptor. These two hydrogen bonds form inversion related R^2_2 (8) dimers (Fig. 4(a), Table 2). These dimers are linked by C−H···O hydrogen bonds involving H_{14} hydrogen atom and the sulfonyl oxygen atom O_{34} to form a double C (7) chains propagating along the c-axis direction and forming a ribbon like architecture (Fig. 4(a)). Neighbouring ribbons are linked via offset π … π interactions [*Cg* … *Cg* = 3.9058 (19) Å; interplanar

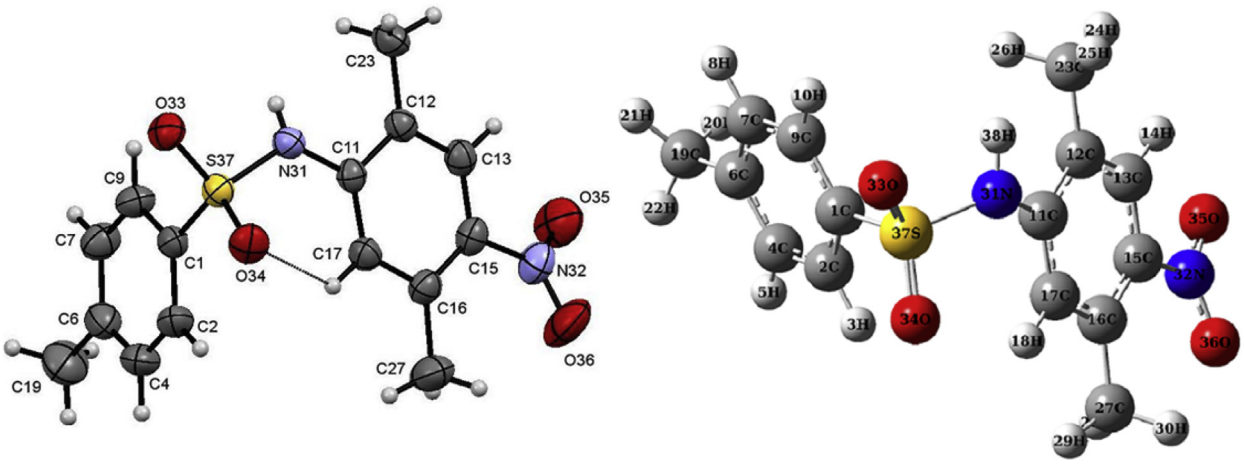

Fig. 3. ORTEP diagram of *N*-(2,5-dimethyl-4-nitrophenyl)-4-methylbenzenesulfonamide with thermal ellipsoids drawn at 50% probability with optimized geometry.

Table 2
Geometric parameters for hydrogen bonds and other intermolecular contacts (Å, °) operating in the crystal structures of NDMPMBS.

D-H … A	D-H	H … A	D … A	D-H … A
C17–H18···O34[a]	0.93	2.45	3.0825	125
N31–H38···O33[b]	0.81	2.20	2.9772	160
C13–H4···O34[c]	0.93	2.38	3.2133	149

[a] Intra.
[b] x,1-y,1-z.
[c] x,y,-1+z.

distance = 3.6104 (19) Å; slippage = 1.490 Å; symmetry code: 1-x,1-y, 1-z] between the nitro aniline rings $C_{11}/C_{12}/C_{13}/C_{15}/C_{16}/C_{18}$ forming a two dimensional sheet parallel to the *ac*-plane, as illustrated in Fig. 4(b).

3.2. Hirshfeld surface analysis

The Hirshfeld surfaces of title compound display in Fig. 5(a), the surfaces have been mapped over d_{norm} (A), shape index (B) and curvedness (C) in the range of −0.452 to 1.427 Å, −1.0 to 1.0 Å and −4.0 to 0.4 Å, respectively. Two major interactions are observed, first interaction between sulfonamide $N_{31}–H_{38}$ with O_{33} of sulphonamide, which can visualize as dark red areas and labelled as a and a'. Another, interaction between O_{34} of sulfonamide with the $C_{13}–H_4$ of nitrobenzene, which can be seen as bright red spots marked as b and b' in Fig. 5(a) and (b), on the d_{norm} mapped surfaces. The upper spike denoted with b (Fig. 5(c)) corresponds to the donor spike (H_{38} atom in SO_2NH group interacting with O_{33} atom of the SO_2NH group), with the lower spike indicate with a corresponding to an acceptor spike (O_{33} atom of the SO_2NH group with H_{38} atom of the SO_2NH group), both are look like sharp spikes with almost same in length and forming inversion dimers that enclose R^2_2 (8) loops. Fig. 5(c), depicted H···H contacts appears as spikes, indicate with red circle and the wings encircled with black due to the C···H contacts. From the fingerprint analysis revealed that the H–H (36.5%) and O–H (36.4%) and C–H (17.6%) contacts appears to be a predominant contribution in the crystal packing.

3.3. Optimized geometry

Full geometry optimization (shown in Fig. 3) of title compound was carried out for isolated molecules in gas phase at DFT/B3LYP/6–311++G (d,p) method, initially coordinates obtained from X-ray

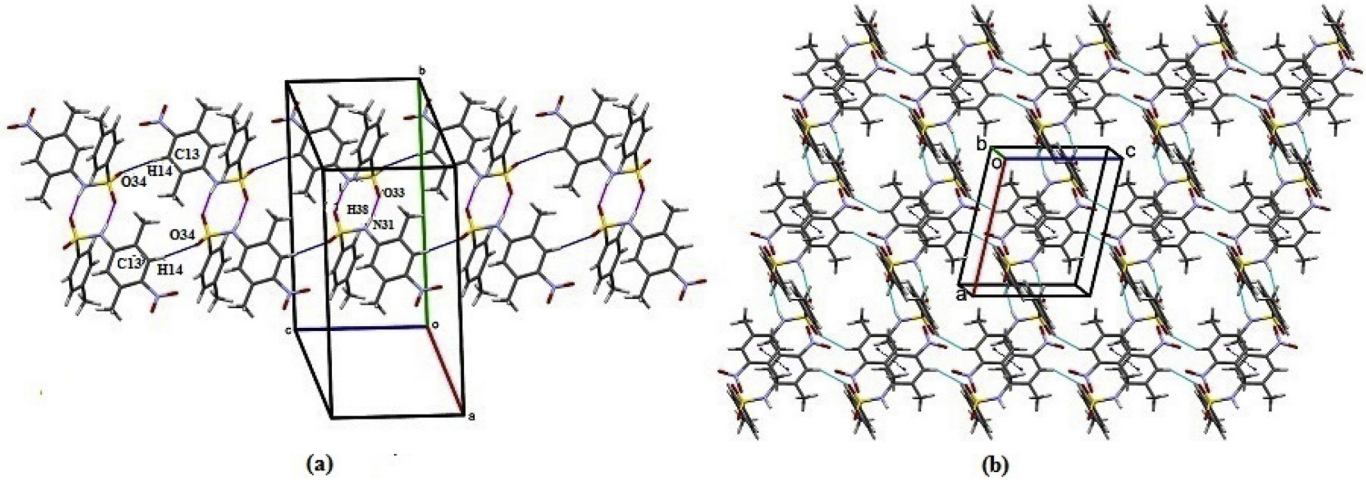

Fig. 4. (a) Ribbon like architecture formed via N–H–O and C–H–O hydrogen bonds in the title compound. (b) A view of the crystal packing of the compound displaying two dimensional sheets.

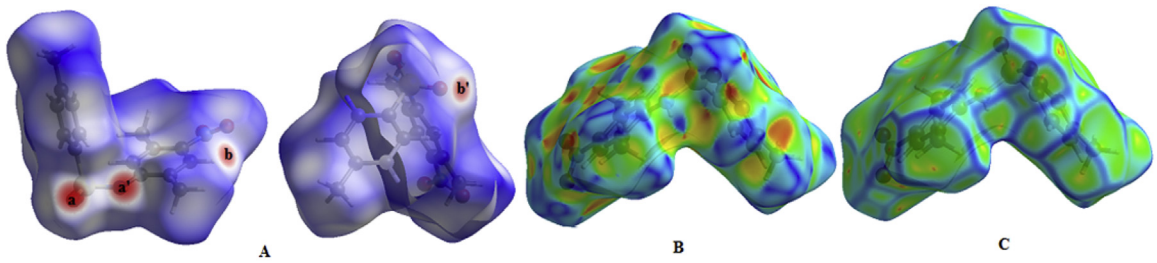

(a) Hirshfeld surfaces of NDMPMBS (A) d_{norm} (B) shape index and (C) curvedness

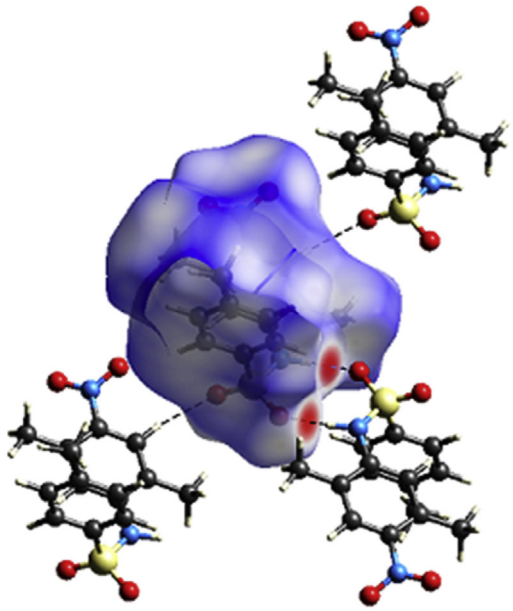

(b) Hirshfeld surfaces mapped with d_{norm} showing various interactions with surrounding molecules

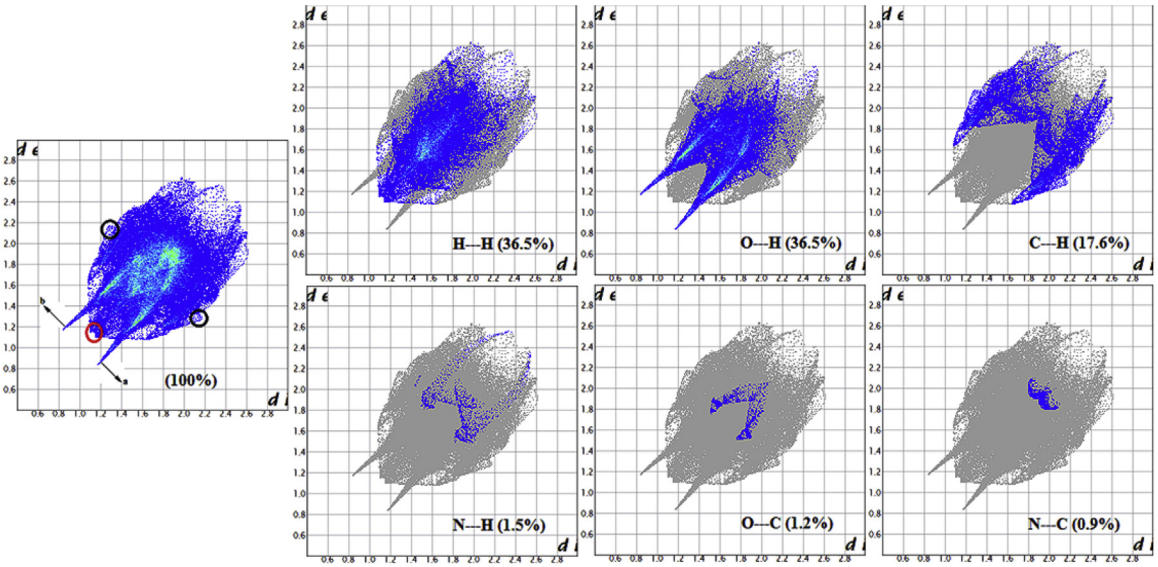

(c) Finger print plots of NDMPMBS; (a) total surface area (100%), (b) H---H (36.5%), (c) O---H (36.4%), (d) C---H (17.6%), N---H(1.5%), O---C(1.2%) and N---C(0.9%) interactions visualized with percentage of contacts.

Fig. 5. (a) Hirshfeld surfaces of NDMPMBS (A) d_{norm} (B) shape index and (C) curvedness. (b) Hirshfeld surfaces mapped with d_{norm} showing various interactions with surrounding molecules. (c) Finger print plots of NDMPMBS; (a) total surface area (100%), (b) H—H (36.5%), (c) O—H (36.4%), (d) C—H (17.6%), N—H (1.5%), O—C (1.2%) and N—C (0.9%) interactions visualized with percentage of contacts.

structure without any constraints. Selected geometrical parameters (bond length (Å), bond angle (°) and torsion angle (°) of investigated compound are listed in Table 3). The comparative study shows a good agreement among the computational and experimental parameters (Supplementary information). The computational geometrical parameters are slightly more than that of experimental values. Because of, the experimental results were based on molecules in the solid state, while the computed values were carried in gas phase for isolated molecule.

3.4. Vibrational spectral analysis

The calculated (scaled) wavenumbers, experimental IR, Raman bands and assignments are given in Table 4.

The N–H stretching vibration mode generally measured in region 3500-3300 cm^{-1} [60,61]. In the present case, the bands observed at 3277 cm^{-1} (IR), 3276 cm^{-1} (Raman) and 3488 cm^{-1} (DFT) is assigned as NH stretching vibration mode. The mode (mode no 1) is pure and PED is exactly 100%. The difference between computational and experimental N–H stretching vibration is 171 cm^{-1} for IR and 172 cm^{-1} for Raman, this may due to the N–H–O intermolecular interaction of title molecule in crystal state. The N–H in-plane bending vibration mode is usually expected around 1400 cm^{-1} [17]. In the present case, the bands observed at 1386 cm^{-1} in the IR spectrum, 1384 cm^{-1} in the Raman spectrum and 1391 cm^{-1} for DFT (B3LYP) are assigned to the N–H in plane bending vibration mode, this is good agreement with literature values. The mode number 79 have calculated wave number at 492 cm^{-1} correlate well with experimental Raman spectrum at 493 cm^{-1} assigned as NH out-of-plane bending vibration.

The asymmetric and symmetric stretching modes of the methyl group are expected in the regions 3000 ± 50 cm^{-1} and 2900 ± 45 cm^{-1} [62,63]. For the title compound the stretching modes are assigned at 2981 cm^{-1} (Raman), in the range 2999–2940 cm^{-1} (B3LYP) (asymmetric stretching modes); 2924 cm^{-1} (IR), 2925 cm^{-1} (Raman) and in the region 2929-2895 cm^{-1} (B3LYP) (symmetric stretching modes) as expected. The asymmetric and symmetric deformations vibrations of methyl group generally appear in the region of 1400–1485 cm^{-1} and 1380-1420 cm^{-1}, respectively [64–67]. For title compound, the bands calculated at 1449, 1435, 1434, 1432, 1430, 1421 cm^{-1} (B3LYP), experimentally observed at 1448, 1418 cm^{-1} (IR) (asymmetric deformation) and 1367, 1363, 1362 cm^{-1} (B3LYP) (symmetric deformation vibrations), shows good agreement with literature values. For the investigated compound, the rocking modes of methyl group are calculated at 1023, 1021, 1017 and 970 cm^{-1} (B3LYP) and experimentally observed at 970 cm^{-1} in the Raman spectrum, assigned as expected. The CH_3 torsion vibrational modes are usually appear in the region 185 ± 65 cm^{-1} [62], the bands assigned at 206, 188, 168 and 28 cm^{-1} (B3LYP).

The stretching vibration modes of aromatic nitro group are expected in range, 1570-1485 cm^{-1} (asymmetric stretching) and 1370-1320 cm^{-1} (symmetric stretching) [68]. For in case of investigated compound, these modes are assigned at 1521, 1502 cm^{-1} (IR), 1520, 1502 cm^{-1} (Raman), 1541, 1505 cm^{-1} (B3LYP) (asymmetric stretching modes); 1300 cm^{-1} (IR and Raman), 1305 cm^{-1} (DFT) (symmetric stretching modes). Both the modes show high IR intensity and Raman activity. The NO_2 deformation modes (scissoring, out-of-plane wagging, in-plane rocking and torsion) are expected in the regions 855 ± 40, 760 ± 30, 540 ± 30 and 70 ± 20 cm^{-1} respectively [62]. The bands at 858, 734 cm^{-1} in IR spectrum, 857, 734 cm^{-1} in Raman spectrum and 847 and 732 cm^{-1} (DFT) are assigned as deformation modes of NO_2 group of title compound. The reported values of the NO_2 deformations modes are 809, 727, 524 cm^{-1} (experimentally), 800, 727, 534 cm^{-1} (DFT) [69].

The asymmetric and symmetric stretching vibrational modes fall in region 1330-1295 cm^{-1} and 1150-1125 cm^{-1}, respectively for SO_2 group [70]. In the present case, the bands computed at 1267 and 1082 cm^{-1} (DFT), experimentally observed at 1260, 1086 cm^{-1} in the IR spectrum and 1260 and 1085 cm^{-1} in the Raman spectrum are assigned as SO_2 asymmetric and symmetric stretching modes. The SO_2 stretching mode is not pure, but it contains contribution from other modes. Although the region of the SO_2 scissoring (560 ± 40 cm^{-1}) and that of SO_2 wagging vibration mode (500 ± 55 cm^{-1}) partly overlap, the two vibrations appear separately [62]. The DFT calculation of these bands at 567 cm^{-1} and 515 cm^{-1}, observed at 566 cm^{-1} and 515 cm^{-1} in the Raman spectrum assigned as wagging and scissoring, respectively. The twisting vibrational mode of SO_2 is fall in region 400 ± 50 cm^{-1} and rocking vibrational mode at around 350 cm^{-1} [62]. For the present case, these modes are computed at 426 cm^{-1} and 255 cm^{-1}, respectively.

The SN stretching vibration modes are expected in region 905 ± 30 cm^{-1} [62] and in present study, the bands observed at 798 cm^{-1} (IR), 797 cm^{-1} (Raman) and 801 cm^{-1} (B3LYP) assigned as these modes. The PED is 33% with IR intensity (145.02) and Raman activity (44.11) respectively. From the references the CN stretching vibration modes are fall in the region 1275 ± 55 cm^{-1} [62], for the title compound the vibrational modes expected at 1337, 1017 cm^{-1}(IR), 1336, 1015 cm^{-1} (Raman) and 1349, 1225, 1017 cm^{-1} (theoretically). The stretching vibration modes for CS generally lie in the region 930-670 cm^{-1} [71]. The CS stretching vibrational wave number for title compound calculated at 629 cm^{-1} and experimentally observed at 632 cm^{-1} (IR and Raman) as expected [71], PED of 21% and with high IR intensity (147.45) and low Raman activity (19.42).

The C–H stretching vibrational modes of substituted benzene ring are generally observed in the region 3000-3100 cm^{-1} [62]. In present case, the C–H modes are assigned at 3102, 3084, 3059 cm^{-1} (IR) and 3101, 3077, 3059, 3045 cm^{-1} (Raman) and 3088, 3087, 3086, 3075, 3050, 3046 cm^{-1} (B3LYP) as expected. The stretching vibration modes (2–7) are pure with PED contribution around 100%. The in-plane and out-of-plane aromatic CH deformation

Table 3
Geometrical parameters of the NDMPMBS.

Bond length (Å) DFT/XRD			
C1–C2	1.393/1.386	S37–N31	1.706/1.636
C1–C9	1.394/1.386	C11–N31	1.410/1.414
C2–C4	1.391/1.380	C11–C17	1.397/1.390
C4–C6	1.399/1.382	C12–C11	1.411/1.400
C6–C7	1.401/1.385	C12–C13	1.386/1.381
C7–C9	1.390/1.376	C15–N32	1.472/1.467
C1–S37	1.794/1.756	C15–C16	1.406/1.387
S37–O33	1.457/1.435	C16–C17	1.396/1.392
S37–O34	1.456/1.423		
Bond angle (°) DFT/XRD			
C1–S37–O33	108.510/108.80	S37–C1–C2	119.732/120.56
C1–S37–O34	107.940/108.54	S37–C1–C9	119.139/118.75
S37–N31–H38	109.049/111.41	C2–C1–C9	121.127/120.69
O33–S37–O34	122.550/119.34	C1–C2–C4	118.954/118.86
O33–S37–N31	102.979/104.14	C2–C4–C6	121.265/121.53
O34–S37–N31	107.449/108.40	C4–C6–C7	118.424/118.42
N31–S37–C1	106.296/106.95		
Torsion angle (°) DFT/XRD			
O33–S37–C1–C2	−155.788/-134.76	N31–S37–C1–C9	−85.795/-65.94
O33–S37–C1–C9	24.365/45.99	S37–C1–C2–C4	−179.096/-178.98
O34–S37–C1–C2	−20.975/-3.45	C9–C1–C2–C4	0.746/0.3
O34–S37–C1–C9	159.178/177.30	S37–C1–C9–C7	179.146/179.23
N31–S37–C1–C2	94.050/113.31		

Table 4
Calculated scaled wave numbers, observed IR and Raman bands and assignment of NDMPMBS.

B3LYP/6–311++G (d,p)			IR	Raman	Assignments[a]
ν(cm^{-1})	IRI	RA	ν(cm^{-1})	ν(cm^{-1})	
3448	46.4581	91.8182	3277	3276	νNH(100)
3088	0.5718	96.5058	3102	3101	νCHII(74)
3087	3.3703	9.074	–	–	νCHII(69)
3086	0.9234	42.5747	3084	–	νCHI(90)
3075	1.4139	82.2193	–	3077	νCHI(93)
3050	7.0118	78.9474	3059	3059	νCHI(95)
3046	9.4734	104.0429	–	3045	νCHI(93)
2999	15.0176	55.4886	–	3000	νasyCH3
2995	10.2853	57.2905	–	–	νasyCH3
2990	11.0976	68.4502	–	–	νasyCH3
2986	5.5996	78.0916	–	2981	νasyCH3
2964	15.5323	86.467	–	–	νasyCH3
2940	13.0716	65.2499	–	–	νasyCH3
2929	11.5999	210.3946	2924	2925	νsyCH3
2909	16.7402	282.9166	–	–	νsyCH3
2895	20.7788	210.3411	–	–	νsyCH3
1596	72.8545	123.5693	–	1595	νPhII(25)
1571	23.4981	71.5686	1572	1573	νPhI(30), δPhI(10)
1549	2.4327	6.3037	–	–	νPhI(27), δPhI(13)
1541	130.8072	150.8671	1521	1520	νasyNO2(11), νPhII(23)
1505	223.5909	57.7494	1502	1502	νasyNO2(30)
1469	69.7658	12.3407	–	–	δCHII(26)
1463	9.1238	1.7324	1453	–	δCHI(20)
1449	11.8096	3.2022	1448	–	δasyCH3(29)
1435	11.8435	6.6691	–	–	δasyCH3(30), τCH3(13)
1434	14.2335	9.1215	–	–	δasyCH3(40), τCH3(12)
1432	10.021	9.273	–	–	δasyCH3(58), τCH39110
1430	22.3058	5.4629	–	–	δasyCH3(27)
1421	8.0846	7.661	1418	–	δasyCH3(53), τCH3(16)
1391	21.8701	1.2362	1386	1384	δHNC (39), δasCH3 (12), νPhII(12)
1372	8.3958	1.4436	–	–	δCH(10), PhI(17)
1367	7.9481	17.2254	–	–	δsyCH3(53)
1363	10.179	8.8532	–	–	δHNC (10), δsyCH3(41)
1362	3.3186	22.9263	–	–	δsyCH3(28)
1349	30.6472	12.2288	1337	1336	νCN(10), PhII(18)
1305	479.1206	466.0533	1301	1300	νsyNO2(36), δNO2(11)
1289	20.1009	4.1237	–	–	νPhII(12)
1283	3.887	11.5492	1283	–	δCHI(13), νPhI(14)
1278	2.8038	3.9597	1278	1278	δCHI(13), νPhI(10)
1267	92.2633	5.4774	1260	1260	νSO2(24), νCHII(16)
1236	57.3095	122.7941	–	–	νSO2(27), νCHII(26)
1225	159.3669	260.7209	–	–	νPhII(13), νCN(14)
1181	2.706	17.4604	–	–	δPhI(12), νCC(39)
1165	9.701	2.0068	–	–	δCHII(13)
1160	4.3426	4.3912	1156	1151	δCHI(17), CC(10)
1124	5.4554	10.3407	–	1124	δPhII(10), νCN(13), νCC(12)
1095	6.9218	0.1308	1089	1089	δCH(15), νPhI(14)
1082	228.657	57.5833	1086	1085	νSO2(27), νCS(12)
1036	49.2109	12.0904	–	–	νSO2(17), νPhI(18)
1023	21.2059	4.1252	–	–	δCH3(16)
1021	25.9912	3.4665	–	–	δCH3(16)
1017	138.9511	52.8199	–	–	δCH3(11), νCN(13), νCC(15)
1017	1.868	0.872	1017	1015	δCH3(11), νCN(13)
1006	23.1045	23.1076	–	–	τHCCC(20)
991	8.8863	2.0952	–	–	δPhI(22)
971	5.1592	7.7547	–	–	νPh(11), τHCCC(19)
970	0.1598	0.2327	–	971	δCH3(10), δCH3(10), τHCCC(36)
954	0.0298	0.3556	–	–	δCHI(23)
935	0.3507	0.3669	–	–	δCHI(18), τPhI(10)
896	33.6547	0.3834	895	895	δCHII(40)
879	5.5845	1.8665	–	–	δCHII(43)
847	2.6101	23.6678	858	857	δNO2(30)
818	0.179	0.262	818	817	δCHI(26)
801	145.0279	44.1127	798	797	νSN(33)
795	53.2133	13.1022	–	–	δCHI(24)
780	38.8255	9.2131	–	–	δNO2(25), δCC(19), δPhII(19)
777	6.191	57.6339	–	–	δPhI(30)
732	5.1162	1.4291	734	734	δNO2
712	6.0197	4.593	706	–	δNO2
697	19.2976	7.6921	–	698	τPhII(16)
688	3.337	1.0984	–	684	τPhI(31)
635	17.125	15.7566	–	–	νPhII(15)
629	147.4525	19.4248	632	632	νCC(14), δPhI(10), νCS(21)

Table 4 (*continued*)

B3LYP/6–311++G (d,p)			IR	Raman	Assignments[a]
ν(cm^{-1})	IRI	RA	ν(cm^{-1})	ν(cm^{-1})	
621	2.5455	6.1092	615	–	νPhI(36)
584	14.7141	0.8446	–	–	τHCCC(12), δCCCC(14)
567	80.959	10.0026	–	566	δSO2 wag (10)
537	88.1423	7.5126	–	–	δONC(14)
515	78.0052	2.5205	–	515	δSO2 sci (14)
492	25.7815	14.2137	–	493	δNHCC(54)
474	2.3793	3.7152	–	–	δCCCC(15)
457	1.7323	10.4594	–	–	νCC(10), δPhII(17)
443	10.9643	2.065	–	–	τPhII(24), δCCCC(12)
426	6.5447	2.3866	–	–	δSO2(28), δCCC(10)
409	0.3637	1.7107	–	–	δCCC(11)
398	0.0749	0.0283	–	–	τPhI(28), τHCCC(12)
383	0.0748	1.8542	–	–	δONC(10), δCCC(15)
355	1.4186	0.4892	–	–	δNSC(12)
320	1.1514	0.8876	–	–	δNSC(11), δCCCC(10)
316	1.0446	0.3568	–	–	δCCC(49)
306	1.7845	0.1186	–	301	νCN(12), δPhII(13)
275	2.1131	5.4593	–	–	νCS(32)
255	3.0132	3.4884	–	–	δSO2 rock (10), νCS(12), δOSN(10)
244	1.7079	2.4539	–	–	δCCN(14), δOSN(19)
227	0.6907	3.3657	–	227	νPhII(10), δCCC(20), νSN(14)
212	1.7256	1.5674	–	–	δNCC(42), δOSN(10)
206	0.7871	0.4177	–	–	τCH3(25), δCCCC(14)
188	1.3078	1.3333	–	–	τCH3(11), δNCCC(15), δNSC(14)
168	0.5755	0.8188	–	–	τCH3(18), δNSC(10)
156	0.7665	0.569	–	–	δSCC(56), δONCS(24)
142	0.3113	0.1023	–	–	τPhII(12), δNCCC(12)
101	3.3054	1.2104	–	–	δCNS(31), δCCN(23)
91	1.9723	0.6841	–	92	τPhII(13)
57	2.9088	1.2039	–	–	τPhII(21)
34	0.0972	1.5942	–	–	τNO2(53)
28	0.1761	0.9245	–	–	τCH3(34)
26	0.0845	3.4964	–	–	τNO2(22)
19	1.3962	6.4671	–	–	τNO2(10)

[a] ν-stretching; δ-in-plane deformation and out-of-plane deformation; τ-torsion; 2,5-dimethyl 4-nitrophenyl and tosyl ring are represented as PhI and PhII; potential energy distribution is given in brackets (%) in the assignment column.

modes are expected above and below 1000 cm^{-1} [62] and for in the case of investigated compound these modes assigned at 1283, 1278, 1260, 1156, 1089 cm^{-1} (IR), 1278, 1260, 1089 cm^{-1} (Raman), 1283, 1278, 1267, 1236, 1095 cm^{-1} (B3LYP) (in-plane deformation) and at 895, 818 cm^{-1} (IR), 895, 817 cm^{-1} (Raman), 896, 818 cm^{-1} (B3LYP) (out-of-plane deformation). The aromatic ring stretching vibrational modes expected in the region 1615-1260 cm^{-1} [62]. For the investigated compound, the bands experimentally observed at 1572, 1502, 1386, 1278 cm^{-1} (IR), 1595, 1573, 1502, 1384, 1278 cm^{-1} (Raman) and in the range of 1596–1278 cm^{-1} (B3LYP) assigned as these modes.

3.5. NMR spectral analysis

NMR spectroscopy is one of the important and valuable tool for identification of structural and functional groups of the molecules. ^{13}C and ^{1}H NMR chemical shifts values of title compound were recorded in DMSO solvent (TMS as internal standard), calculated in DMSO at GIAO method [72] using DFT/6-311G++(d,p) basic set, which provide information about the number of different types of carbon atoms and the number of different types of protons present in the molecule, respectively. The ^{13}C and ^{1}H NMR spectra are given in Fig. 6(a) and (b). Correlated results of experimental and calculated ^{13}C and ^{1}H NMR chemical shifts values are given in Table 5.

The result in Table 5 shows that the range of ^{13}C NMR chemical shift of typical organic molecule usually is > 100 ppm [73,74] the accuracy ensures reliable interpretation of spectroscopic parameters. In ^{13}C NMR spectrum, upfield signal observed at 16.92, 19.68 and 20.95 ppm and calculated at 16.85, 24.07, 22.09 ppm was assigned to methyl carbon atoms at C_{23}, C_{27} and C_{19}. The signals for aromatic carbons (tosyl ring and nitrobenzene ring) were observed at 126.57–145.12 ppm and calculated at 124.86–154.11 ppm for DFT. The C_{15} carbon of nitrobenzene ring appears 145.12 ppm due to nitro substitution, calculated as 150.35 ppm. The signal at C_1 and C_6 carbons of tosyl ring appears at 137.31 ppm (147.51 ppm) and 139.89 ppm (154.11 ppm) (experimental/calculated) due to methyl group as well as sulfonyl group substitution. The signal at 143.59 ppm is assigned as C_{11} carbon of nitrobenzene ring due to amine group substitution, which was calculated at 149.61 ppm, show good agreement.

The title compound have 16 protons occur in three regions, out of which 9 protons attached to methyl groups, one protons is attached nitrogen (N–H proton) and 6 protons are aromatic protons. The 9 methyl protons are occur in the upfield region at δ 2.04, 2.37, 2.42 ppm (experimental) and calculated at 2.01, 2.35, 2.64 ppm, shows good agreement. The N–H proton observed experimental at 10.01 ppm and computed at 6.07 ppm. The phenyl ring protons are observed around at 7.20–7.82 ppm (experimental) which shows good agreement with calculated value 7.45–8.17 ppm.

3.6. Electronic spectra and frontier molecular orbital analysis

Electronic spectra of title compound calculated in DMSO as well as methanol solution by TD-DFT/PCM model using B3LYP/6-311G++(d,p) basic set (Table 6). The electronic spectra of the title

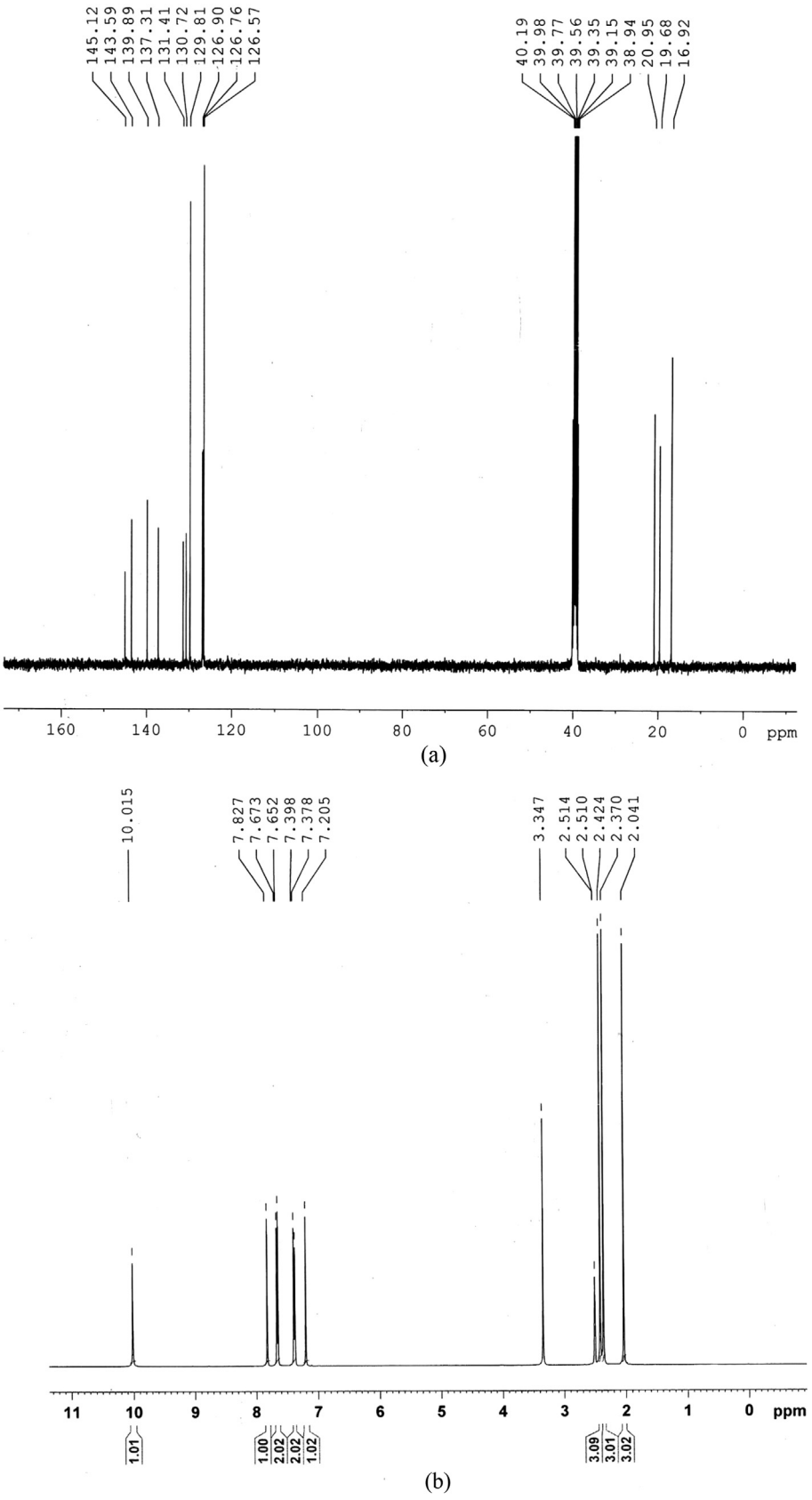

Fig. 6. ^{13}C NMR (a) and ^{1}H NMR (b) spectrum of *N*-(2,5-dimethyl-4-nitrophenyl)-4-methylbenzenesulfonamide.

Table 5
Experimental and calculated (^{13}C and ^{1}H) NMR chemical shifts (ppm) of NDMPMBS.

Atom	Experimental (ppm)	TMS B3LYP/6-311 + G (2d,p) GIAO (ppm)
^{13}C-NMR		
C23	16.92	16.85
C27	19.68	24.07
C19	20.95	22.09
C17	126.57	124.86
C13	126.76	133.47
C12	126.90	131.86
C2, C9	129.81	131.04
C4, C7	130.72	134.71
C16	131.41	144.83
C1	137.31	147.19
C6	139.89	154.11
C11	143.59	149.61
C15	145.12	150.35
^{1}H-NMR		
H24–H26	2.04	2.01[a]
H20–H22	2.37	2.35[a]
H28–H30	2.42	2.64[a]
H5, H8	7.38	7.45[a]
H18	7.20	8.10
H3, H10	7.66	7.82[a]
H14	7.82	8.17
H38	10.01	6.07

[a] Average.

compound (in Figure S2 and S3 supporting information) illustrate an electronic absorption band with maxima at 349 nm (DMSO) and 347 nm (methanol), is due to the electronic transition from the ground state to the first excited state. It is mainly described by one-electron excitation from the HOMO (characterizes by the ability of electron donating) to LUMO (characterizes by the ability of electron accepting). Diagrammatic representation of HOMO-LUMO proved in Fig. 7, HOMO (MO 84) is confined on $-NH-SO_2$ group and delocalized over nitrobenzene; LUMO (MO 85) is confined on nitro group, delocalized on benzene ring of nitrobenzene. Consequently, HOMO→LUMO transition implies an electron cloud transfer from $-SO_2$ group to nitro group through the benzene ring of title compound. In case of title compound, the calculated energy values of HOMO and LUMO are −7.01 eV and −2.7 eV, respectively and the energy separation between HOMO and LUMO is 4.31 eV.

In order to understand the chemical reactivity of title compound, global reactivity parameters were calculated DFT method.

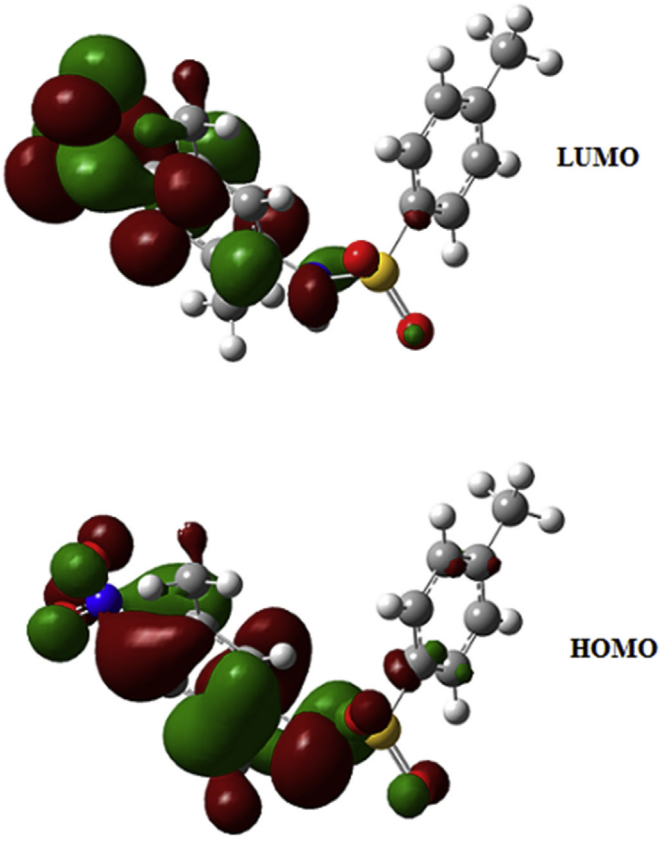

Fig. 7. HOMO-LUMO plots of *N*-(2,5-dimethyl-4-nitrophenyl)-4-methylbenzene sulfonamide.

Single point calculation was performed at DFT at 6–311++G (d,p) method. The difference in energies gave the vertical ionization potential (I) and vertical electron affinity (A) defined by equations, $I = E_{N-1} - E_N$, $A = E_N - E_{N+1}$, where E_{N+1}, E_N and E_{N-1} are the energies of the N+1, N and N-1 electron systems respectively [75]. The magnitude of global reactivity descriptor values as tabulated in Table 7 were calculated with the help of energies of Ionization potential (I) and electronic affinity (A) utilizing equations provided in the supplementary material.

Table 6
Theoretical electronic absorption spectra of title compound (absorption wavelength λ (nm), excitation energies E (eV) and oscillator strengths (*f*)) using TD-DFT/B3LYP/6311++G (d,p) method.

Excitation	CI expansion	Energy Coefficient (eV)	Wavelength (nm)	Oscillator Strength (*f*)
DMSO				
84 → 85	0.68391	3.5498	349	0.3372
80 → 85	0.23487	3.7555	330	0.0277
82 → 85	−0.12971			
83 → 85	0.63785			
80 → 85	0.61136	3.9266	315	0.0317
82 → 85	−0.12639			
83 → 85	−0.25811			
84 → 85	0.15724			
Methanol				
84 → 85	0.68231	3.5631	347	0.3240
80 → 85	0.24398	3.7605	329	0.0255
82 → 85	−0.12914			
83 → 85	0.63440			
80 → 85	0.60688	3.9277	315	0.0330
82 → 85	−0.12481			
83 → 85	−0.26620			
84 → 85	0.16292			

3.7. Local reactivity properties of NDMPMBS – MEP and ALIE surfaces, Fukuifunction surfaces and non-covalent interactions

In order to locate possibly important reactive sites of the newly synthetized NDMPMBS molecule, in this study we have also investigated frequently used quantum-molecular descriptors such as MEP, ALIE and Fukui functions. Values of the aforementioned quantities have been mapped to the electron density surface in order to visualize their distribution within NDMPMBS molecule, Figs. 8–10.

We begin with the identification of possibly important reactive (electrophilic and nucleophilic) sites by the molecular electrostatic potential (MEP) surface, which is a very useful descriptor in studies of biological recognition and hydrogen-bonding interactions [76,77]. The pictorial representation with rainbow colour scheme of electrostatic potential for title compound has been shown in Fig. 8, in the range of −6.012 a. u. to +6.012 a. u. The darkest red colour denotes electron rich regions (V(r) <-6.012 a. u.) that could be sensitive towards electrophilic attacks. According to Fig. 8 these regions are localized over oxygen atoms O_{33} and O_{34} (belonging to sulfonyl group) and oxygen atoms O_{35} and O_{36} (belonging to the nitro group). The darkest blue colour indicates electron poor regions (V(r) > +6.012 a. u.), and therefore the molecule sites that could be sensitive towards the nucleophilic attacks.

Also, the electrostatic potential mapped over the d_{norm} surface of the neighbouring molecules (Figure S4 supporting information) clearly showed that the electrostatic potential on the hydrogen bond donors and acceptors in the neighbouring molecules are to one another (red spots close to H-acceptor and blue spots close to H-bond donors), thus provide further evidence to the R^2_2 (8) hydrogen bond pattern formed by N–H–O hydrogen bonds (Figure S4 supporting information). indicates the occurrence of N_{31}–H_{38}–O_{33}, C_{13}–H_{14}–O_{34} and C_{17}–H_{18}–O_{34} interactions in title compound. ALIE surface is even more reliable tool than MEP for the identification of molecule sites sensitive towards electrophilic attacks, since ALIE values show molecule areas where electrons are least tightly bound [78–81]. Representative ALIE surface (Fig. 9) of NDMPMBS molecule emphasizes the importance of oxygen atoms O_{35} and O_{36}, when it comes to the sensitivity to electrophilic attacks. These molecule sites are characterized by the lowest ALIE values of ~217 kcal/mol. Intramolecular noncovalent interactions have also been visualized in Fig. 9. Two noncovalent interactions were formed between oxygen and hydrogen atoms (O_{34}–H_{18} and O_{36}–H_{30}), with very similar strength of ~0.015 electron/bohr^3.

The importance of oxygen atoms O_{35} and O_{36} from the aspect of reactivity has been also confirmed by Fukui functions as well, Fig. 10. Fukui functions give information about the changes in electron density as a consequence of charge addition or removal. Purple color in Fig. 10(a) gives information about where electron density increased after the charge addition, while negative color in Fig. 10(b) gives information where electron density decreased after the charge addition. According to the results presented in Fig. 10(a), electron density could increase in the near vicinity of oxygen atoms O_{36} and O_{37} after the charge addition. On the other side, results in Fig. 10(b) indicate that electron density decreases in the near vicinity of oxygen atoms O_{33} and O_{34} after the charge removal.

Table 7
The energy values of global reactivity descriptors (Ionization potential (IP), electron affinity (EA), electro negativity (χ), chemical potential (μ), global hardness (η), global softness (σ) and global electrophilicity (ω)) for title compound.

Parameter	Value (eV)
Ionization potential (IP)	8.48
Electron affinity (EA)	1.09
Electronegativity (χ)	4.78
Chemical potential (μ)	−4.78
Global hardness (η)	3.69
Global softness (σ)	0.13
Electrophilicity index (ω)	3.09

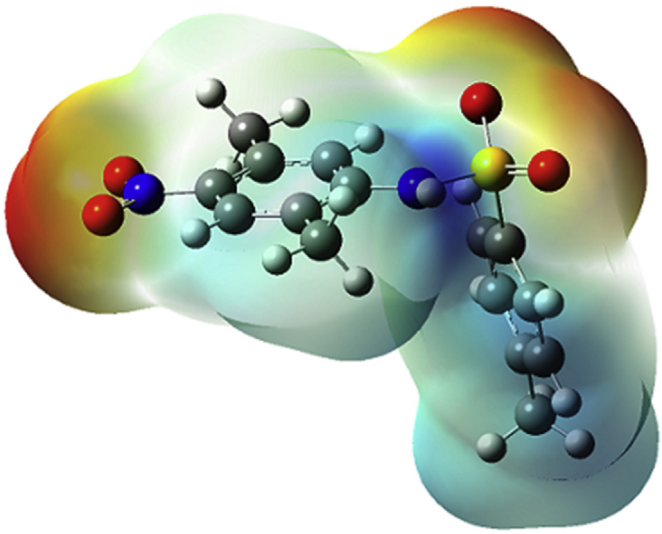

Fig. 8. MEP plot of *N*-(2,5-dimethyl-4-nitrophenyl)-4-methylbenzenesulfonamide.

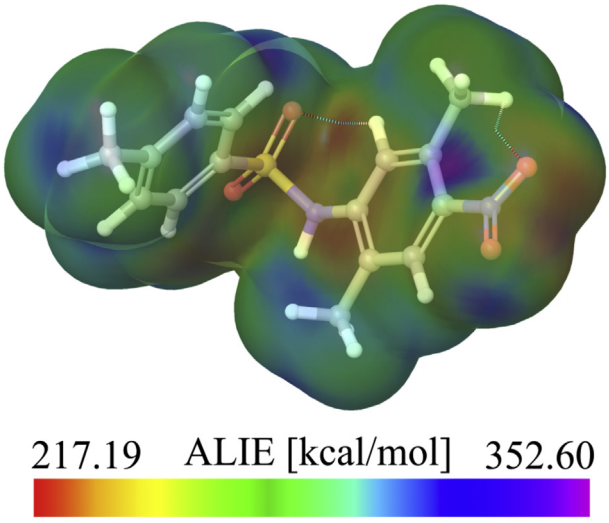

Fig. 9. Representative of ALIE surface of *N*-(2,5-dimethyl-4-nitrophenyl)-4-methylbenzenesulfonamide.

3.8. Nonlinear optical properties

Nonlinear optical materials occupy a foremost function in nonlinear optics and in particular they have a great impact on information technology and industrial applications. NLO properties find applications in optical communication, telecommunications, optical phase conjugation, frequency mixing, optical mixing, dynamic image processing, signal processing and second harmonic wave generation [82–84]. Total dipole moment (μ_o), anisotropy of the polarizability (α_{tot}), mean polarizibility ($\Delta\alpha$), and first-order hyperpolarizibilitiy(β) of NDMPMBS were calculated at DFT/B3LYP/6-311G++(d,p) method and listed in Table 8. The dipole moment and mean polarizability of the title compound are 2.2670

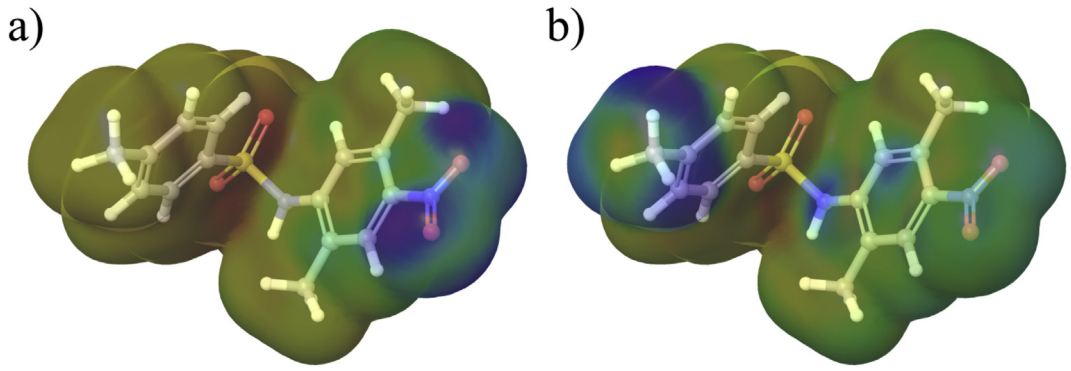

Fig. 10. Fukui functions of *N*-(2,5-dimethyl-4-nitrophenyl)-4-methylbenzenesulfonamide.

Debye and 7.4165 × 10^{-24} esu. The is first-order hyperpolarizibilitiy(β) of NDMPMBS calculated and is found to be 12.02 × 10^{-30} esu which is 92.46 times greater than that of the standard NLO material urea (0.13 × 10^{-30} esu) [85]. The highest value of first-order hyperpolarizibilitiy(β) may be due transfer of π-electron cloud from donor (sulphonamide group) to acceptor (nitro group) which makes molecule highly polarized and the possibility of intra molecular charge transfer (ICT).

3.9. NBO analysis

The natural bond orbital (NBO) calculations were performed using NBO 3.1 program [86] as executed in the Gaussian09 suite at the B3LYP/6–311++G (d,p) (5D, 7 F) basic set which offers a suitable basis for examining the various interactions in both filled and virtual orbital spaces that could enhance the analysis of inter and intramolecular interactions. The second-order Fock-matrix was carried out to evaluate the donor–acceptor interactions in the NBO basis [87,88]. In NBO analysis large E (2) value shows the intensive interaction between electron-donors and electron-acceptors, and greater the extent of conjugation of the whole system, the possible intensive interaction are given in Tables 9 and 10.

The strong interaction $n_3(O_{35}) \rightarrow \pi^*(N_{32}–O_{36})$ has the highest E (2) value 155.95 kJ/mol and an another interaction has been in $n_1(N_{31}) \rightarrow \pi^*(C_{11}–C_{17})$ with an energy of 23.39 kJ/mol. Table 10 gives the occupancy of electrons and p-character in significant NBO natural atomic hybrid orbital. Almost, a very close to pure p-character was observed in π-bonding of $C_{11}–C_{17}$, $N_{32}–O_{36}$ and lone pairs of n_2O_{33}, n_2O_{34}, n_2O_{35}, n_3O_{35}, n_2O_{36}, n_1N_{31}.

3.10. Mulliken atomic charge analysis

The Mulliken atomic charges of investigated compound calculated at DFT/B3LYP/6-31 + G (d,p) method in gaseous state are given in Table 11. It is based on the linear combination of atomic orbitals and therefore the wave function of the molecule are obtained from Mulliken population analysis [89]. The charge distribution on the molecule has an important role in the application of quantum chemistry calculations for the molecular system.

From the analysis of Table 11, hydrogen atoms of title compound shows atomic charges with positive values in the range of 0.138–0.308 and but some H atoms exhibit more positive atomic charges H_{38} (0.308), H_{14} (0.247) and H_{18} (0.266) comparative other hydrogen atoms and possess acidic nature. Due to the presence of more negative atomic charges values on oxygen atom O_{33} (−0.131), O_{34} (−0.100) and nitrogen atom N_{31} (−0.215), net positive atomic charge values on hydrogen atom H_{38} (0.308), H_{14} (0.247) and H_{18} (0.266) may support the formation of hydrogen bonding $N_{31}–H_{38}–O_{33}$, $C_{13}–H_{14}–O_{34}$ and $C_{17}–H_{18}–O_{34}$.

3.11. Sensitivity towards autoxidation and stability in water

Modern water purification methods in the case of organic pharmaceutical pollutants are based on the oxidation reactions [90–92]. In terms of computational molecular modelling techniques, the concept of bond dissociation energies (BDE) can be useful for predicting molecule's weak spots where degradation could start. Particularly, bond dissociation energies for hydrogen abstraction (H-BDE) resemble the molecule's sensitivity towards autoxidation mechanism [93–95], while in the same time BDEs for the remaining single acyclic bonds can be very useful for predicting

Table 8
The electric dipole moment (μ), polarizability (Δα) and first order hyper polarizability (β) of title compound by B3LYP/6-311G++(d,p).

Parameter	Value	Parameter	a.u.	esu (×10^{-24})	Parameter	a.u.	esu (×10^{-33})
μ_x	−1.7249	α_{xx}	265.9277	39.4104	β_{xxx}	966.0397	8345.9067
μ_y	1.1390	α_{xy}	13.2483	1.9633	β_{xxy}	718.7733	6209.6981
μ_z	0.9312	α_{yy}	217.2198	32.1919	β_{xyy}	322.1631	2783.2636
μ_o	2.2670	α_{xz}	−24.6687	3.6559	β_{yyy}	29.1894	252.1759
		α_{yz}	1.0165	0.1506	β_{xxz}	−137.3283	1186.4203
		α_{zz}	214.6588	31.8124	β_{xyz}	−28.2303	243.89
		α_{tot}	232.6021	34.4716	β_{yyz}	−24.3833	210.6546
		Δα	50.0441	7.4165	β_{xzz}	−120.6461	1042.2978
					β_{yzz}	4.6938	40.5511
					β_{zzz}	77.0165	665.3686
					β_{tot}	1391.7089	12023.3906
					$\beta_{tot} = 12.02 \times 10^{-30}$ esu		

Table 9
Second-order perturbation theory analysis of Fock matrix in NBO basis corresponding to the intramolecular bonds of the title compound.

Donor(i)	Type	ED/e	Acceptor(j)	Type	ED/e	E (2)[a]	E(*j*)-E(i)[b]	F (i,j)[c]
C1–C2	σ	1.97716	C1–C9	σ*	0.02400	3.90	1.27	0.063
_	–		C2–C4	σ*	0.01496	2.13	1.30	0.047
_	–		O33–S37	σ*	0.14580	0.58	0.99	0.022
C1–C9	σ	1.97704	C1–C2	σ*	0.02395	3.89	1.28	0.063
_	–		C7–C9	σ*	0.01480	2.18	1.30	0.048
_	–		O34–S37	σ*	0.15553	0.61	0.99	0.023
C2–C4	σ	1.97568	C1–C2	σ*	0.02395	2.83	1.25	0.053
_	–		C1–S37	σ*	0.20548	3.50	0.86	0.051
_	–		C4–C6	σ*	0.02239	2.55	1.27	0.051
_	–		C6–C19	σ*	0.01388	3.33	1.11	0.054
C4–C6	σ	1.97692	C2–C4	σ*	0.01496	2.33	1.27	0.049
_	–		C6–C7	σ*	0.02266	2.53	1.26	0.050
_	–		C6–C19	σ*	0.01388	1.31	1.11	0.034
C6–C7	σ	1.97678	C4–C6	σ*	0.02239	2.52	1.26	0.050
_	–		C6–C19	σ*	0.01388	1.27	1.11	0.034
_	–		C7–C9	σ*	0.01480	2.34	1.27	0.049
C7–C9	σ	1.97587	C1–C9	σ*	0.02400	2.88	1.25	0.054
_	–		C1–S37	σ*	0.20548	3.38	0.87	0.051
_	–		C6–C7	σ*	0.02266	2.54	1.27	0.051
_	–		C6–C19	σ*	0.01388	3.28	1.12	0.054
C11–C17	σ	1.97383	C11–C12	σ*	0.03083	3.62	1.25	0.060
_	–		C11–N31	σ*	0.03005	0.93	1.12	0.029
_	–		C12–C23	σ*	0.01497	3.23	1.11	0.054
C11–C17	π	1.63339	C11–C17	π*	0.37633	0.76	0.28	0.013
_	–		C12–C13	π*	0.30516	15.53	0.29	0.061
_	–		C15–C16	π*	0.41191	21.46	0.28	0.075
C12–C13	σ	1.97050	C11–C12	σ*	0.03083	3.03	1.25	0.055
_	–		C11–N31	σ*	0.03005	4.14	1.12	0.061
_	–		C12–C23	σ*	0.01497	1.70	1.11	0.039
C15–C16	σ	1.97351	C13–C15	σ*	0.01906	3.79	1.27	0.062
_	–		C16–C17	σ*	0.01780	2.11	1.28	0.047
_	–		C16–C27	σ*	0.01377	1.71	1.12	0.039
N32–O36	σ	1.99561	C13–C15	σ*	0.01906	0.80	1.62	0.032
_	–		C15–N32	σ*	0.09523	0.55	1.36	0.025
N32–O36	π	1.98387	C15–C16	π*	0.41191	3.35	0.46	0.039
_	–		N32–O36	π*	0.63887	7.42	0.31	0.052
LP N31	σ	1.80373	C1–S37	σ*	0.20548	7.63	0.47	0.053
_	–		C11–C17	π*	0.37633	23.39	0.33	0.082
_	–		O34–S37	σ*	0.15553	3.69	0.57	0.042
LP O33	σ	1.98241	C1–S37	σ*	0.20548	0.81	0.96	0.026
_	–		O34–S37	σ*	0.15553	2.20	1.07	0.045
LP O33	π	1.81651	C1–S37	σ*	0.20548	17.99	0.45	0.081
_	–		N31–S37	σ*	0.27315	8.97	0.40	0.055
LP O34	σ	1.98051	C1–S37	σ*	0.20548	0.77	0.96	0.026
_	–		O33–S37	σ*	0.14580	2.08	1.07	0.043
LP O34	π	1.81923	C1–S37	σ*	0.20548	17.63	0.45	0.080
_	–		N31–S37	σ*	0.27315	10.34	0.40	0.059
LP O35	σ	1.9813	C15–N32	σ*	0.09523	4.27	1.09	0.062
_	–		N32–O36	σ*	0.63887	2.27	1.21	0.047
LP O35	π	1.89823	C15–N32	σ*	0.09523	11.51	0.58	0.073
_	–		N32–O36	σ*	0.05723	19.09	0.70	0.104
LP O35	n	1.46754	N32–O36	π*	0.63887	155.95	0.14	0.136
LP O36	π	1.90136	C15–N32	σ*	0.09523	10.94	0.58	0.071
_	–	–	N32–O35	σ*	0.05831	19.69	0.70	0.106

[a] E (2) means energy of hyper-conjugative interactions (stabilization energy in kJ/mol).
[b] Energy difference (a.u) between donor and acceptor i and j NBO orbitals.
[c] F (i,j) is the Fock matrix elements (a.u) between i and j NBO orbitals.

where degradation mechanism could start.

Since majority of pharmaceutical pollutants eventually end up in the water resources, it is also of great importance for predictions of degradation properties to understand the stability of molecules in water. This can be done thanks to the molecular dynamics (MD) simulations and radial distribution functions (RDF), which are very useful for the identification of atoms with pronounced interactions with water molecules. The results regarding BDEs are presented in Fig. 11, while Fig. 12 contains information on the most important RDFs.

Results presented in Fig. 11 indicate the absence of H-BDE values lower than at least 90 kcal/mol. This indicates that the title

Table 10
NBO results showing the formation of Lewis and non-Lewis orbitals.

Bond (A-B)	ED/e[a]	EDA%	EDB%	NBO	s%	p%
σC1-C2	1.97716	51.40	48.60	0.7169 ($sp^{1.61}$)C+	38.33	61.63
_	−0.74770	–	–	0.6971 ($sp^{1.97}$)C	33.65	66.30
σC1-C9	1.97704	51.34	48.66	0.7165 ($sp^{1.63}$)C+	38.05	61.91
_	−0.74669	–	–	0.6975 ($sp^{1.97}$)C	33.66	66.29
σC2-C4	1.97568	50.33	49.67	0.7094 ($sp^{1.81}$)C+	35.52	64.44
_	−0.72622	–	–	0.7048 ($sp^{1.86}$)C	35.00	64.96
σC4-C6	1.97692	49.28	50.72	0.7020 ($sp^{1.85}$)C+	35.03	64.93
_	−0.72233	–	–	0.7121 ($sp^{1.94}$)C	34.00	65.96
σC6-C7	1.97678	50.68	49.32	0.7119 ($sp^{1.95}$)C+	33.84	66.12
_	−0.72114	–	–	0.7023 ($sp^{1.86}$)C	34.97	64.99
σC7-C9	1.97587	49.65	50.35	0.7046 ($sp^{1.85}$)C+	35.09	64.87
_	−0.72850	–	–	0.7096 ($sp^{1.80}$)C	35.66	64.30
σC11-C17	1.97383	51.47	48.53	0.7174 ($sp^{1.71}$)C+	36.88	63.08
_	−0.73082	–	–	0.6966 ($sp^{1.97}$)C	33.65	66.30
πC11-C17	1.63339	47.40	52.60	0.6885 ($sp^{99.99}$)C+	0.01	99.99
_	−0.28039	–	–	0.7252 ($sp^{99.99}$)C	0.01	99.95
σC12-C13	1.97050	50.80	49.20	0.7127 ($sp^{1.86}$)C+	35.00	64.96
_	−0.72910	–	–	0.7014 ($sp^{1.80}$)C	35.76	64.20
σC15-C16	1.97351	50.44	49.56	0.7102 ($sp^{1.60}$)C+	38.44	61.52
_	−0.73156	–	–	0.7040 ($sp^{2.03}$)C	33.01	66.95
σN32-O36	1.99561	49.06	50.94	0.7004 ($sp^{2.15}$)N+	31.66	68.23
_	−1.08213	–	–	0.7138 ($sp^{3.13}$)O	24.18	75.68
πN32-O36	1.98387	39.14	60.86	0.6256 ($sp^{99.99}$)N+	0.02	99.72
_	−0.45651	–	–	0.7801 ($sp^{99.99}$)O	0.06	99.71
n1 N31	1.80373	–	–	$sp^{14.60}$	6.41	93.56
_	−0.32731	–	–	–	–	–
n1 O33	1.98241	–	–	$sp^{0.32}$	75.47	24.50
_	−0.82036	–	–	–	–	–
n2 O33	1.81651	–	–	$sp^{99.99}$	0.08	99.61
_	−0.31360	–	–	–	–	–
n1 O34	1.98051	–	–	$sp^{0.33}$	75.20	24.76
_	−0.81948	–	–	–	–	–
n2 O34	1.81923	–	–	$sp^{99.99}$	0.11	99.58
_	−0.31566	–	–	–	–	–
n1O35	1.98139			$sp^{0.32}$	75.71	24.28
_	−0.81272	–	–	–	–	–
n2 O35	1.89823	–	–	$sp^{99.99}$	0.25	99.64
_	−0.29882	–	–	–	–	–
n3O35	1.46754	–	–	$sp^{99.99}$	0.07	99.73
_	−0.28319	–	–	–	–	–
n2O36	1.90136	–	–	$sp^{99.99}$	0.41	99.48
_	−0.30047	–	–	–	–	–

[a] ED/e is expressed in a. u.

Table 11
Mulliken atomic charge of title compound by DFT/B3LYP/6-311G (d,p).

Atoms	Atomic charges	Atoms	Atomic charges
S37	0.134	H3	0.208
N31	−0.215	H5	0.182
N32	−0.203	H8	0.184
O33	−0.131	H10	0.249
O34	−0.100	H14	0.247
O35	0.013	H18	0.266
O36	0.004	H20	0.185
C1	0.204	H21	0.151
C2	−0.285	H22	0.156
C4	−0.610	H24	0.175
C6	0.496	H25	0.182
C7	−0.495	H26	0.153
C9	−0.164	H28	0.195
C11	−0.199	H29	0.138
C12	0.955	H30	0.212
C13	−0.442	H38	0.308
C15	−2.057		
C16	1.860		
C17	−0.683		
C19	−0.479		
C23	−0.471		
C27	−0.326		

molecule is not sensitive towards the autoxidation mechanism. Namely, all of the H-BDE values are much higher than the desired threshold of 90 kcal/mol, with the lowest H-BDE values calculated for hydrogen atoms of methyl groups, thanks to which it is expected that the title molecule is stable in the presence of oxygen. The lowest BDE value of the rest of the single acyclic bonds have been calculated in the case of N—S bond, with BDE value of just 41 kcal/mol, indicating that degradation could start precisely by breaking of this bond. Other significantly low BDE values have been calculated in the cases of C—N bond (N belonging to the NO_2 group) and C—S bond, with BDE values of around 70 kcal/mol, indicating that detachment of benzene or NO_2 group could occur during the degradation.

Calculations of RDFs indicate that six atoms of NDMPMBS have high and sharp RDF curves. However, five of six of the aforementioned atoms have their maximal g(r) values located at distances of around 4 Å. Certainly, the most important RDF has been calculated in the case of hydrogen atom H_{38}, with its maximal g(r) value located at distance of 2 Å, which indicates significant interactions with water molecules. This hydrogen atom with the most important RDF curve is located adjacent to the bond with the lowest BDE value, indicating that the influence of water could be of importance for the degradation of NDMPMBS.

3.12. Drug likeness and molecular docking

Drug likeness properties associated to the Lipinski's rule of five [96,97] for the newly synthetized NDMPMBS molecule have been calculated and summarized in Table 12. According to all parameters provided in Table 12 it can be concluded that newly synthetized NDMPMBS molecule could be considered as a candidate for practical applications in some pharmaceutical formulation. Namely, the AlogP value is 3.67, which is far below the desired threshold of 5. In the same time, prospective drug candidates should have less than 5 and 10 HBD and HBA, respectively. These prerequisites are also fulfilled by the NDMPMBS molecule. Ghose et al. [98], have stated that the molar refractivity should be in the range between 40 and 130, while PSA should take values less than 140 $Å^2$. Inspection of Table 12 clearly indicates that these criteria are satisfied by the NDMPMBS molecule, including the criteria by Veber et al. [99], for the number of rotatable bonds, which should be lower than 10. NDMPMBS molecule is also very close to satisfy the Congreeve's rule of three [100]. Namely, the Congreeve's rule of three is just slightly violated by the NDMPMBS molecule in terms of somewhat higher AlogP value and one more rotatable bond.

Drug likeness parameters motivated us to further investigate NDMPMBS molecule from the aspect of pharmaceutical properties. In order to identify in which direction NDMPMBS molecule could exhibit its biological activity we have employed the Prediction of Activity Spectra for Substances (PASS) online software [101], which screens the biologically activity spectrum of the potential drug candidates taking into account the large training set. The results concerning the predicted biological activities have been summarized in Table 13, where Pa represents the probability for molecule to be active, while Pi represents the probability for molecule to be inactive. Table 13 contains information about activities that are higher than 0.7.

According to the screening of biological activities by PASS it can be seen that NDMPMBS molecule has significantly high probabilities to be active as inhibitor of arylsulfatesulfotransferase and

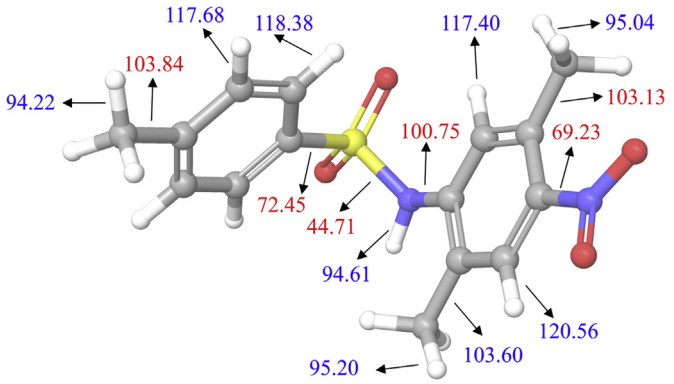

Fig. 11. BDE of all single acyclic bonds of *N*-(2,5-dimethyl-4-nitrophenyl)-4-methylbenzenesulfonamide.

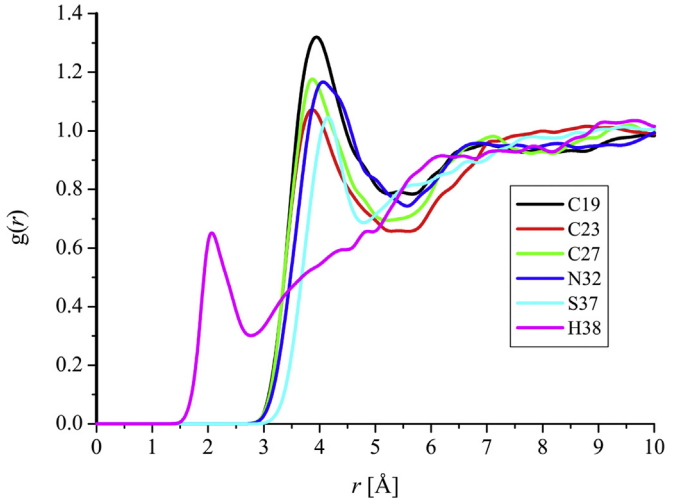

Fig. 12. RDF's of atoms of *N*-(2,5-dimethyl-4-nitrophenyl)-4-methylbenzenesulfonamide with significant interactions with water.

Table 12
Drug likeness parameters for the NDMPMBS molecule.

Descriptor	Value
Hydrogen Bond Donor (HBD)	1
Hydrogen Bond Acceptor (HBA)	2
Mass	320.40
AlogP	3.67
Polar surface area (PSA) [Å2]	97.69
Molar refractivity	85.34
Number of atoms	38
Number of rotatable bonds	4

polyporopepsin. Since probabilities for these two activities are very similar, we have decided to investigate how NDMPMBS molecule binds to the representatives of proteins related to arylsulfate-sulfotransferase and polyporopepsin. Using the RCSB protein databank and taking into account the arylsulfatesulfotransferase and polyporopepsin inhibitor acitivites we have chosen to investigate docking of NDMPMBS to proteins with PDB IDs: 1WKR and 3ETT, respectively.

Molecular docking has been performed with Autodock4 tools, while preparation of ligand and proteins has been performed with AutoDock tools [102]. After being imported from the protein databank, proteins have been firstly prepared by the set of the

Table 13
PASS predicted biological activities of NDMPMBS.

Pa	Pi	Activity
0.889	0.004	Arylsulfate sulfotransferase inhibitor
0.888	0.007	Polyporopepsin inhibitor
0.860	0.005	Glutamyl endopeptidase II inhibitor
0.850	0.003	Phospholipid-translocating ATPase inhibitor
0.766	0.011	Omptin inhibitor
0.757	0.010	Venombin AB inhibitor
0.744	0.003	Antiprotozoal (Coccidial)
0.758	0.023	Benzoate-CoA ligase inhibitor
0.731	0.004	Aspergillopepsin I inhibitor
0.724	0.011	2-Hydroxymuconate-semialdehyde hydrolase inhibitor
0.734	0.056	Ubiquinol-cytochrome-c reductase inhibitor

actions including: removal of water molecules, addition of hydrogen atoms and addition of charges according to Gasteiger-Marsili approach. Protein sites which contained docked molecules from the experimentally obtained results were used as a target search space for docking studies. Fig. 13 contains illustration of the docked NDMPMBS molecule to the surface of the two selected proteins, while binding energies of several representative docking modes have been summarized in Table 14.

Results provided in Fig. 13 and Tables 12–14 indicate great potential of the newly synthesized NDMPMBS molecule for application in pharmaceutical applications. Fig. 13 and Table 14 illustrate that NDMPMBS molecule binds to 1WKR and 3ETT proteins with significantly high binding energies. In both cases binding energy of the most representative docking mode had the value of −7.20 kcal/

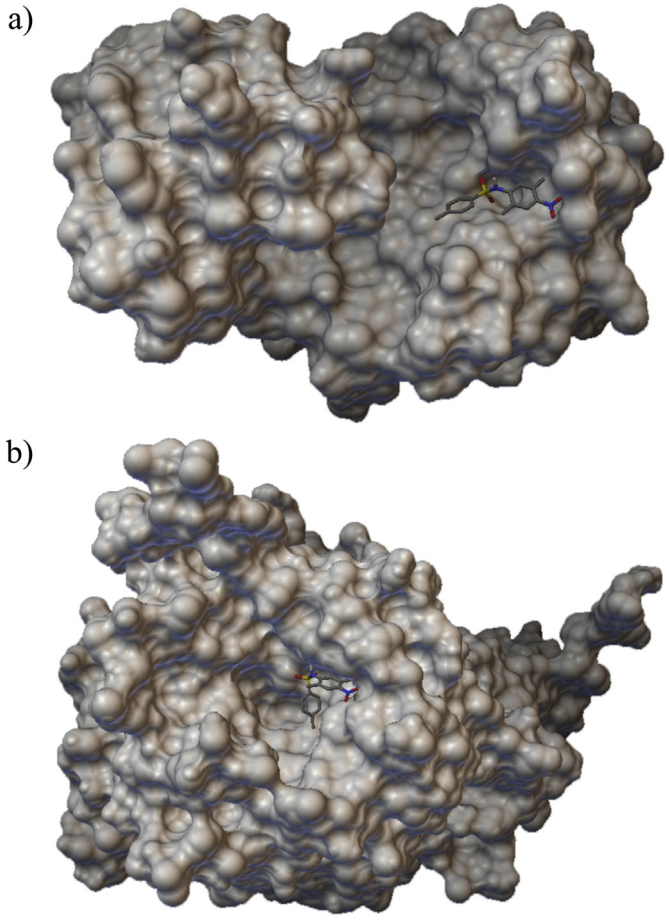

Fig. 13. Docked NDMPMBS molecule at the surface of a) 1WKR and b) 3ETT proteins.

Table 14
The binding energies of several modes for docking of NDMPMBS against 1WKR and 3ETT

Mode	Binding energy with 1WKR (kcal/mol)	Binding energy with 3ETT (kcal/mol)
1	−7.20	−7.20
2	−6.96	−7.12
3	−6.90	−7.12
4	−5.77	−7.01
5	−5.76	−6.97
6	−5.70	−6.85
7	−5.62	−6.78
8	−5.61	−6.66
9	−5.46	−6.97
10	−5.45	−6.79

mol. However, the remaining docking modes in the case of 3ETT protein had higher magnitudes of binding energies than in the case of 1WKR protein. Thus, the molecular docking results indicate that the newly synthetized molecule could be considered as a candidate with significant activity against the bacterial arylsulfatesulfotransferase catalytic intermediate (3ETT).

4. Conclusion

N-(2,5-dimethyl-4-nitrophenyl)-4-methylbenzenesulfonamide has been synthesized and characterized by single crystal X-ray diffraction, FT-IR, FT-Raman, ^{1}H and ^{13}C NMR. The molecular conformation is stabilized by $C_{17}—H_{18}—O_{34}$ intra-molecular hydrogen bond that encloses to form a S (6) motif. The vibrational spectroscopic studies of title compound were investigated experimentally (FT-IR and FT-Raman) and theoretically. The complete assignment of normal mode of vibrations was done by potential energy distribution analysis. Computationally predicted geometrical parameters are good in agreement with the experimental SCXRD data. HOMO is confined on $—NH—SO_2$ group and delocalized over nitrobenzene; LUMO is confined on nitro group, delocalized on benzene ring of nitrobenzene which gives charge transfer process in the molecular system. The most electrophilic sites are oxygen atoms of sulfonyl group as well as nitro group and neucleophilic sites are amine hydrogen as well as other hydrogen atoms. The is first-order hyperpolarizibilitiy(β) of NDMPMBS calculated and is found to be 12.02×10^{-30} esu which is 92.46 times that of the standard NLO material urea. ALIE surfaces and Fukui functions indicate that oxygen atoms O_{35} and O_{36} could be important reactive centres of the NDMPMBS molecule. H-BDE values indicate that NDMPMBS molecule is not sensitive towards the autoxidation, however BDE of the N—S bond has very low value of just 41 kcal/mol, indicating that degradation mechanism could start with the breaking of this bond. Analysis of RDFs indicate that hydrogen atom H_{38} has pronounced interactions with water molecules, which could be also of importance for the degradation of NDMPMBS molecule, since H_{38} is adjacent to the weakest single acyclic bond. Drug likeness parameters indicate high potential of the title molecule for the practical pharmaceutical applications.

Acknowledgments

The authors are highly thankful to the UGC for financial assistance. Authors are grateful to Prof. K. Saraswathi, Dept. of Chemistry, S.V.University, Tirupati for her constant support and encouragement. The authors are highly thankful to Professor V.R. Pedireddi, Solid State & Supramolecular Structural Chemistry Laboratory, School of Basic Sciences, IIT Bhubaneswar for the collection of diffraction data. Part of this work has been performed thanks to the support received from Schrödinger Inc. Part of this study was conducted within the projects supported by the Ministry of Education, Science and Technological Development of Serbia, grant numbers OI 171039 and TR 34019.

Appendix A. Supplementary data

Supplementary data related to this article can be found at https://doi.org/10.1016/j.molstruc.2017.10.028.

References

[1] C. Hansch, P.G. Sammes, J.B. Taylor, Comprehensive Medicinal Chemistry, vol. 2, Pergamon Press, Oxford, 1990 (Chapter 7).1.
[2] Kelly Chibale, Hayley Haupt, Howard Kendrick, Vanessa Yardley, Ahilan Saravanamuthu, Alan H. Fairlamb, Simon L. Croft, Antiprotozoal and cytotoxicity evaluation of sulfonamide and urea analogues of quinacrine, Bioorg. Med. Chem. Lett. 11 (2001) 2655.
[3] S.S. Stokes, R. Alber, E.T. Buurman, B. Andrews, A.B. Shapiro, O.M. Green, A.R. McKenzie, L.R. Otterbein,Inhibitors of the acetyltransferase domain of N-acetylglucosamine-1-phosphate-uridylyltransferase/glucosamine-1-phosphate-acetyltransferase (GlmU). Part 2: optimization of physical properties leading to antibacterial aryl sulfonamides, Bioorg. Med. Chem. Lett. 23 (2012) 7019–7023.
[4] A. Hanafy, J. Uno, H. Mitani, Y. Kang, Y. Mikami, Vitro antifungal activities of sulfa drugs against clinical Isolates of Aspergillus and Cryptococcus species, Jpn. J. Med. Mycol. 48 (1) (2007) 47–50.
[5] Chester M. Himal, Wissam G. Aboul-Saad, J. Agr. Food. Chem. 19 (6) (1971) 1175–11580.
[6] J.F. Kennedy, M. Thorley, Pharmaceutical Substances, thi[rd] ed., A. Kleeman, J. Engel, B. Kutscher, D. Reichert, Thieme, Stuttgart, 1999.
[7] D. Vullo, V. De Luca, A. Scozzafava, V. Carginale, M. Rossi, C.T. Supuran, C. Capasso, The extremo-α-carbonic anhydrase from the thermophilic bacterium Sulfurihydrogenibiumazorense is highly inhibited by sulphonamides, Bioorg Med. Chem. 21 (15) (2013) 4521–4525.
[8] J.I. Levin, J.M. Chen, M.T. Du, F.C. Nelson, L.M. Killar, S. Skala, A. Sung, G. Jin, R. Cowling, D. Barone, C.J. March, K.M. Mohler, R.A. Black, J.S. Skotnicki, Anthranilatesulfonamidehydroxamate TACE inhibitors. Part 2: SAR of the acetylenic P1′ group, Bioorg Med. ChemLett. 12 (8) (2002) 1199–1202. http://www.sciencedirect.com/science/article/pii/S0960894X02001361.
[9] William R. Roush, Stephen L. Gwaltney , Jianming Cheng, Karl A. Scheidt, James H. McKerrow, Elizabeth Hansell, Vinyl sulfonateesters and vinyl sulfonamides: potent, irreversible inhibitors of cysteine proteases, J. Am. Chem. Soc. 120 (42) (1998) 10994–10995.
[10] J. Mun, A.A. Jabbar, N.S. Devi, S. Yin, Y. Wang, C. Tan, D. Culver, J.P. Snyder, Van E.G. Meir, M.M. Goodman, Design and in-vitro activities of N-alkyl-N-[(8-R-2,2-dimethyl-2H-chromen-6-yl)methyl]heteroarylsulfonamides, novel, small-molecule hypoxia inducible factor-1 pathway inhibitors and anticancer agents, J. Med. Chem. 55 (2012) 6738–6750.
[11] N.S. El-Sayed, E.R. El-Bendary, S.M. El-Ashry, M.M. El-Kerdawy, Synthesis and antitumor activity of new sulfonamide derivatives of thiadiazolo[3,2-a]pyrimidines, Eur. J. Med. Chem. 46 (2011) 3714–3720.
[12] E. De Clercq, New developments in anti-HIV chemotherapy, Curr. Med. Chem. 8 (2001) 1543–1572.
[13] N. Hirayama, J. Taga, S. Oshima, T. Honjo, Sulfonamide-type di-schiff base ligands as chelate extraction reagents for divalent metal cations, Anal. ChimActa 466 (2002) 295–301.
[14] E.G.C. Clarke, A.C. Moffat (Eds.), Clarke's Isolation and Identification of Drugs, The Pharmaceutical Press, London, 1986.
[15] S.C. Chaturvedi, S.H. Mishra, K.L. Bhargava, Indian Drugs 17 (1980) 367.
[16] J.D. Xing, T. Zeng, 4-methyl-N-(4-nitrophenyl)benzenesulfonamide, Acta-Cryst E61 (2005) o4318–o4319.
[17] K. Sarojini, H. Krishnan, C.C. Kanakam, S. Muthu, Synthesis, structural, spectroscopic studies, NBO analysis, NLO and HOMO-LUMO of 4-methyl-N-(3-nitrophenyl)benzene sulfonamide with experimental and theoretical approaches, Spectrochim. Acta 108A (2013) 159–170.
[18] T. Rajamani, S. Muthu, M. Karabacak, Electronic absorption, vibrational spectra, nonlinear optical properties, NBO analysis and thermodynamic properties of N-(4-nitro-2-phenoxyphenyl) methanesulfonamide molecule by ab initio HF and density functional methods, Spectrochim. Acta 108A (2013) 186–196.
[19] K. Govindarasu, E. Kavitha, N. Sundaraganesan, Synthesis, structural, spectral (FT-IR, FT-Raman, UV, NMR), NBO and first order hyperpolarizability analysis of N-phenylbenzenesulfonamide by density functional theory, Spectrochim. Acta 133A (2014) 417–431.
[20] S.R. Sebastian, M.I. Attia, M.S. Almutairi, A.A. El-Emam, C.Y. Panicker, C. Van Alsenoy, FT-IR, FT-Raman, molecular structure, first order hyperpolarizability, HOMO and LUMO analysis, MEP and NBO analysis of 3-(adamantan-1-yl)-4-(prop-2-en-1-yl)-1H-1, 2, 4-triazole-5 (4H)-thione, a potential bioactive agent, Spectrochim. Acta 132A (2014) 295–304.
[21] F. Yu, J. Ma, D. Bi, Enhanced adsorptive removal of selected pharmaceutical

antibiotics from aqueous solution by activated graphene, Environ. Sci. Pollut. Res. 22 (6) (2015) 4715–4724.
[22] K. Liu, S. Zhang, X. Hu, K. Zhang, A. Roy, G. Yu, Understanding the adsorption of PFOA on MIL-101 (Cr)-based anionic-exchange metal-organic frameworks: comparing DFT calculations with aqueous sorption experiments, Environ. Sci. Technol. 49 (14) (2015) 8657–8665.
[23] T. Wang, X.X. Tian, Y.W. Li, J. Wang, M. Beller, H. Jiao, Coverage-dependent CO adsorption and dissociation mechanisms on iron surfaces from DFT computations, ACS Catal. 4 (6) (2014) 1991–2005.
[24] S. Armaković, S.J. Armaković, S. Koziel, Optoelectronic properties of curved carbon systems, Carbon 111 (2017) 371–379.
[25] S. Armaković, S. Armaković, N. Finčur, F. Šibul, D. Vione, J. Šetrajčić, B. Abramović, Influence of electron acceptors on the kinetics of metoprololphotocatalytic degradation in TiO 2 suspension, A combined experimental and theoretical study, RSC Adv. 5 (67) (2015) 54589–54604.
[26] S.J. Armaković, M. Grujić-Brojčin, M. Šćepanović, S. Armaković, A. Golubović, B. Babić, B.F. Abramović, Efficiency of La-doped TiO2 calcined at different temperatures in photocatalytic degradation of β-blockers, Arabian J. Chem. (2017), https://doi.org/10.1016/j.arabjc.2017.01.001.
[27] S. Armaković, S.J. Armaković, B.F. Abramović, Theoretical investigation of loratadine reactivity in order to understand its degradation properties: DFT and MD study, J. Mol. Model. 22 (10) (2016) 240.
[28] A.A. Taherpour, A. Mozafai, S. Ranjbar, S. Taban, A study of the effects of solvent on structural and conformational properties of ranitidine tautomer forms by DFT method, Struct. Chem. 26 (2) (2015) 517–529.
[29] S.G. Sagdinc, D. Erdas, I. Gunduz, A.E. Sahinturk, FT-IR and FT-Raman spectra, molecular structure and first-order molecular hyperpolarizabilities of a potential antihistaminic drug, cyproheptadine HCl, Spectrochim. Acta 134A (2015) 350–360.
[30] B. Abramović, S. Kler, D. Šojić, M. Laušević, T. Radović, D. Vione, Photocatalytic degradation of metoprolol tartrate in suspensions of two TiO2-based photocatalysts with different surface area. Identification of intermediates and proposal of degradation pathways, J. Hazard. Mater. 198 (2011) 123–132.
[31] O.V. Dolomanov, L.J. Bourhis, R.J. Gildea, J.A.K. Howard, H. Puschmann, OLEX2: a complete structure solution, refinement and analysis program, J. Appl. Cryst. 42 (2009) 339–341.
[32] G.M. Sheldrick, A short history of SHELX, ActaCryst A64 (2008) 112–122.
[33] A.L. Spek, Structure validation in chemical crystallography, ActaCrystallogr., D. 65 (2009) 148–155.
[34] L.J. Farrugia, WinGX suite for small-molecule single-crystal crystallography, J. Appl. Crystallogr. 32 (1999) 837–838.
[35] C.F. Macrae, I.J. Bruno, J.A. Chisholm, P.R. Edgington, P. McCabe, E. Pidcock, L. Rodriguez-Monge, R. Taylor, J. van de Streek, P.A. Wood, Mercury CSD 2.0-new features for the visualization and investigation of crystal structures, J. Appl. Cryst. 41 (2008) 466–470.
[36] A.D. Becke, Density-functional thermochemistry. III. The role of exact exchange, J. Chem. Phys. 98 (7) (1993) 5648–5652.
[37] M.J. Frisch, G.W. Trucks, H.B. Schlegel, G.E. Scuseria, M.A. Robb, J.R. Cheeseman, G. Scalmani, V. Barone, B. Mennucci, G.A. Petersson, H. Nakatsuji, M. Caricato, X. Li, H.P. Hratchian, A.F. Izmaylov, J. Bloino, G. Zheng, J.L. Sonnenberg, M. Hada, M. Ehara, K. Toyota, R. Fukuda, J. Hasegawa, M. Ishida, T. Nakajima, Y. Honda, O. Kitao, H. Nakai, T. Vreven, J.A. Montgomery Jr., J.E. Peralta, F. Ogliaro, M. Bearpark, J.J. Heyd, E. Brothers, K.N. Kudin, V.N. Staroverov, T. Keith, R. Kobayashi, J. Normand, K. Raghavachari, A. Rendell, J.C. Burant, S.S. Iyengar, J. Tomasi, M. Cossi, N. Rega, J.M. Millam, M. Klene, J.E. Knox, J.B. Cross, V. Bakken, C. Adamo, J. Jaramillo, R. Gomperts, R.E. Stratmann, O. Yazyev, A.J. Austin, R. Cammi, C. Pomelli, J.W. Ochterski, R.L. Martin, K. Morokuma, V.G. Zakrzewski, G.A. Voth, P. Salvador, J.J. Dannenberg, S. Dapprich, A.D. Daniels, O. Farkas, J.B. Foresman, J.V. Ortiz, J. Cioslowski, D.J. Fox, Gaussian 09, Revision B.01, Gaussian, Inc., Wallingford CT, 2010.
[38] R. Dennington, T. Keith, J. Millam, Gaussview, Semichem Inc., Shawnee-Mission, KS, 2009, version 5. .
[39] Michal H. Jamroz, Vibrational Energy Distribution Analysis VEDA4, Warsaw, 2004-2010.
[40] Pittsburg, PA J.B. Foresman, in: E. Frisch (Ed.), Exploring Chemistry with Electronic Structure Methods: a Guide to Using Gaussian, 1996.
[41] A.D. Bochevarov, E. Harder, T.F. Hughes, J.R. Greenwood, D.A. Braden, D.M. Philipp, D. Rinaldo, M.D. Halls, J. Zhang, R.A. Friesner, Int. J. Quantum Chem. 113 (2013) 2110–2142.
[42] D. Shivakumar, J. Williams, Y. Wu, W. Damm, J. Shelley, W. Sherman, J. Chem. Theor. Comput. 6 (2010) 1509–1519.
[43] Z. Guo, U. Mohanty, J. Noehre, T.K. Sawyer, W. Sherman, G. Krilov, Chem. Biol. Drug Des. 75 (2010) 348–359.
[44] K.J. Bowers, E. Chow, H. Xu, R.O. Dror, M.P. Eastwood, B.A. Gregersen, J.L. Klepeis, I. Kolossvary, M.A. Moraes, F.D. Sacerdoti, Scalable algorithms for molecular dynamics simulations on commodity clusters, in: SC 2006 Conference, Proceedings of the ACM/IEEE, IEEE, 2006.
[45] Materials Science Suite 2017-2, Schrödinger, LLC, New York, NY, 2017.
[46] E. Harder, W. Damm, J. Maple, C. Wu, M. Reboul, J.Y. Xiang, L. Wang, D. Lupyan, M.K. Dahlgren, J.L. Knight, OPLS3: a force field providing broad coverage of drug-like small molecules and proteins, J. Chem. Theory Comput. 12 (1) (2015) 281–296.
[47] W.L. Jorgensen, D.S. Maxwell, J. Tirado-Rives, Development and testing of the OPLS all-atom force field on conformational energetics and properties of organic liquids, J. Am. Chem. Soc. 118 (45) (1996) 11225–11236.
[48] W.L. Jorgensen, J. Tirado-Rives, The OPLS [optimized potentials for liquid simulations] potential functions for proteins, energy minimizations for crystals of cyclic peptides and crambin, J. Am. Chem. Soc. 110 (6) (1988) 1657–1666.
[49] H.J. Berendsen, J.P. Postma, W.F. van Gunsteren, J. Hermans, Interaction models for water in relation to protein hydration, in: B. Pullman (Ed.), Intermolecular Forces, Reidel, Dordrecht, 1981, pp. 331–342.
[50] A. Otero-de-la-Roza, E.R. Johnson, J. Contreras-García, Revealing non-covalent interactions in solids: NCI plots revisited, Phys. Chem. Chem. Phys. 14 (2012) 12165–12172.
[51] E.R. Johnson, S. Keinan, P. Mori-Sanchez, J. Contreras-Garcia, A.J. Cohen, W. Yang, Revealing noncovalent interactions, J. Am. Chem. Soc. 132 (2010) 6498–6506.
[52] M.A. Spackman, D. Jayatilaka, CrystEngComm 11 (2009) 19–32.
[53] F.L. Hirshfeld, Theor. Chim. Acta 44 (1977) 129–138.
[54] H.F. Clausen, M.S. Chevallier, M.A. Spackman, B.B. Iversen, New J. Chem. 34 (2010) 193–199.
[55] A.L. Rohl, M. Moret, W. Kaminsky, K. Claborn, J.J. McKinnon, B. Kahr, Cryst. GrowthDes 8 (2008) 4517–4525.
[56] A. Parkin, G. Barr, W. Dong, C.J. Gilmore, D. Jayatilaka, J.J. McKinnon, M.A. Spackman, C.C. Wilson, CrystEngComm 9 (2007) 648–652.
[57] M.A. Spackman, J.J. McKinnon, CrystEngComm 4 (2002) 378–392.
[58] P.A. Wood, J.J. McKinnon, S. Parsons, E. Pidcock, M.A. Spackman, CrystEngComm 10 (2008) 368.
[59] S.K. Wolff, D.J. Grimwood, J.J. McKinnon, D. Jayatilaka, M.A. Spackman, Crystal Explorer 3.1, University of Western Australia, Perth, Australia, 2012. http://hirshfeldsurfacenet.blogspot.com.
[60] L.J. Bellamy, The IR Spectra of Complex Molecules vol. 1, John Wiley and Sons, NY, 1975.
[61] A. Spire, M. Barthes, H. Kallouai, G. De Nunzio, Far-infrared spectra of acetanilide revisited, Phys. D. 137 (2000) 392–401.
[62] N.P.G. Roeges, Guide to the Interpretation of Infrared Spectra of Organic Structure, John Wiley & Sons Inc., New York, 1994.
[63] G. Socrates, Infrared Characteristic Group Frequencies, John Wiley & Sons Inc., New York, 1981.
[64] G. Varsanyi, Assignment of Vibrational Spectra of Seven Hundred Benzene Derivatives, Wiley, New York, 1974.
[65] J.F. Arenas, I. LópezTocón, J.C. Otero, J.I. Marcos, Vibrational spectrum of 2-methylpyridine, J. Molstruct. 410 (1997) 443–446.
[66] F. Márquez, I. LópezTocón, J.C. Otero, J.I. Marcos, A priori SQM vibrational spectrum of 2,2′-bipyridine, J. Molstruct. 410 (1997) 447–450.
[67] J.F. Arenas, Juan T. López-Navarrete, Juan I. Marcos, Juan C. Otero, Vibrational spectrum and internal rotation in 2-methylpyrazine, J. Chem. Soc. Faraday Trans. 2 (84) (1988) 53–65.
[68] V. Krishna Kumar, V. Balachandran, FTIR and FT-Raman spectra assignments anddensity functional calculations of 2,6-dibromo-4-nitroaniline and 2-(mrthylthio)aniline, Spectrochim. Acta 61A (2005) 1811–1819.
[69] C.Y. Panicker, L. UshaKumari, T. Ertan, I. Yildiz, C.M. Granadeiro, H.I.S. Nogueira, Y.S. Mary, FT-IR, FT-Raman, SERS spectra and Computational calculations of 4-Ethyl-N-(2'-hydroxy-5'-nitrophenyl)benzamide, J. Raman Spectrosc. 41 (2010) 381–390.
[70] L.J. Bellamy, The Infrared Spectra of Complex Molecules, vol. 2, Chapman and Hall, London, 1980.
[71] Y. Miyamoto, K. Kaifu, T. Koyano, M. Saito, M. Kato, Second harmonic generation from mixed Langmuir-Blodgett films of N-acyl-p-nitroaniline and its homologous amphiphile, Thin Solid Films 210–211 (1992) 178–181.
[72] R. Ditchfield, Molecular orbital theory of magnetic shielding and magnetic susceptibility, J. Chem. Phys. 56 (1972) 5688–5691.
[73] H.O. Kalinowski, S. Brawn, Carbon13 NMR Spectroscopy, John Wiley and Sons, Chichester, 1988.
[74] K. Pinlajer, E. Kleinpeter (Eds.), Carbon13 Chemical Shifts in Structure and Spectrochemical Analysis, VCH publishers, Deerfield Beach, 1994.
[75] F. De Proft, N. Sablon, D.J. Tozer, P. Geerlings, Calculation of negative electron affinity and aqueous anion hardness using kohn-Sham HOMO and LUMO energies, Faraday Discuss. 135 (2007) 151.
[76] E. Scrocco, J. Tomasi, Electronic molecular structure, reactivity and intermolecular forces: an euristic interpretation by means of electrostatic molecular potentials, Adv. Quantum Chem. 11 (1979) 115–193.
[77] N. Okulik, A.H. Jubert, Theoretical analysis of the reactive sites of non-steroidal anti-inflammatory drugs, Internet Electron, J. Mol. Des. 4 (2005) 17–30.
[78] J.S. Murray, J.M. Seminario, P. Politzer, P. Sjoberg, Average local ionization energies computed on the surfaces of some strained molecules, Int. J. Quantum Chem. 38 (S24) (1990) 645–653.
[79] P. Politzer, F. Abu-Awwad, J.S. Murray, Comparison of density functional and Hartree–Fock average local ionization energies on molecular surfaces, Int. J. quantum Chem. 69 (4) (1998) 607–613.
[80] F.A. Bulat, A. Toro-Labbé, T. Brinck, J.S. Murray, P. Politzer, Quantitative analysis of molecular surfaces: areas, volumes, electrostatic potentials and average local ionization energies, J. Mol. Model. 16 (11) (2010) 1679–1691.
[81] P. Politzer, J.S. Murray, F.A. Bulat, Average local ionization energy: a review, J. Mol. Model. 16 (11) (2010) 1731–1742.
[82] D.S. Bradsshow, D.L. Andrews, Quantum channels in nonlinear optical

processes, j. Nonlinear opt. Phys. Materials 18 (2009) 285–299.
[83] M.N. Arshad, A.M. Al-Dies, A.M. Asiri, M. Khalid, A.S. Birinji, K.A. Al-Amry, A.A.C. Braga, Synthesis, crystal structures, spectroscopic and nonlinear optical properties of chalcone derivatives: a combined experimental and theoretical study, J. Mol. Struct. 1141 (2017) 142–156.
[84] M. Adeel, A.A.C. Braga, M.N. Tahir, F. Haq, M. Khalid, M.A. Halim, Synthesis, X-ray crystallographic, spectroscopic and computational studies of Amino-thiazole derivatives, Synth. J. Mol. Struct. 1131 (2017) 136–148.
[85] C. Adant, M. Dupuis, J.L. Bredas, Ab initio study of the nonlinear optical properties of urea, electron correlation and dispersion effects, Int. J. Quantum Chem. 56 (2004) 497–507.
[86] E.D. Glendening, A.E. Reed, J.E. Carpenter, F. Weinhold, NBO, Gaussian Inc., Pittsburgh, PA, 2003, Version 3.1. .
[87] M.N. Tahir, M. Khalid, A. Islam, S.M.A. Mashhadi, A.A.C. Braga, Facile synthesis, single crystal analysis, and computational studies of sulphanilamide derivatives, J. Mol. Struct. 1127 (2017) 766–776.
[88] S. Naseem, M. Khalid, M.N. Tahir, M.A. Halim, A.A.C. Braga, M.M. Naseer, Z. Shafiq, Synthesis, structural, DFT studies, docking and antibacterial activity of a xanthene based hydrazone ligand, J. Mol. Struct. 1143 (2017) 235–244.
[89] R.S. Mulliken, Electronic population analysis on LCAO–MO molecular wave functions. I, J. Chem. Phys. 23 (1955) 1833–1840.
[90] S.W. Hovorka, C. Schöneich, Oxidative degradation of pharmaceuticals: theory, mechanisms and inhibition, J. Pharm. Sci. 90 (3) (2001) 253–269.
[91] K.A. Connors, G.L. Amidon, V.J. Stella, Chemical Stability of Pharmaceuticals: a Handbook for Pharmacists, John Wiley & Sons, 1986.
[92] D. Johnson, L. Gu, Autoxidation and antioxidants, Encycl. Pharm. Technol. 1 (1986) 415–449.
[93] P. Lienard, J. Gavartin, G. Boccardi, M. Meunier, Predicting drug substances autoxidation, Pharm. Res. 32 (1) (2015) 300–310.
[94] J.S. Wright, H. Shadnia, L.L. Chepelev, Stability of carbon-centered radicals: effect of functional groups on the energetics of addition of molecular oxygen, J. Comput. Chem. 30 (7) (2009) 1016–1026.
[95] T. Andersson, A. Broo, E. Evertsson, Prediction of drug candidates' sensitivity toward autoxidation: computational estimation of C- H dissociation energies of carbon-centered radicals, J. Pharm. Sci. 103 (7) (2014) 1949–1955.
[96] C.A. Lipinski, F. Lombardo, B.W. Dominy, P.J. Feeney, Experimental and computational approaches to estimate solubility and permeability in drug discovery and development settings, Adv. drug Deliv. Rev. 23 (1–3) (1997) 3–25.
[97] C.A. Lipinski, Lead-and drug-like compounds: the rule-of-five revolution, Drug Discov. Today Technol. 1 (4) (2004) 337–341.
[98] A.K. Ghose, V.N. Viswanadhan, J.J. Wendoloski, A knowledge-based approach in designing combinatorial or medicinal chemistry libraries for drug discovery. 1. A qualitative and quantitative characterization of known drug databases, J. Comb. Chem. 1 (1) (1999) 55–68.
[99] D.F. Veber, S.R. Johnson, H.-Y. Cheng, B.R. Smith, K.W. Ward, K.D. Kopple, Molecular properties that influence the oral bioavailability of drug candidates, J. Med. Chem. 45 (12) (2002) 2615–2623.
[100] M. Congreve, R. Carr, C. Murray, H. Jhoti, A 'rule of three'for fragment-based lead discovery? Drug Discov. today 8 (19) (2003) 876–877.
[101] D. Filimonov, A. Lagunin, T. Gloriozova, A. Rudik, D. Druzhilovskii, P. Pogodin, V. Poroikov, Prediction of the biological activity spectra of organic compounds using the PASS online web resource, Chem. Heterocycl. Compd. 50 (3) (2014) 444–457.
[102] O. Trott, A.J. Olson, AutoDock Vina: improving the speed and accuracy of docking with a new scoring function, efficient optimization and multithreading, J. Comput. Chem. 31 (2010) 455–461.